NASA TECHNICAL NOTE

NASA TN D-2689

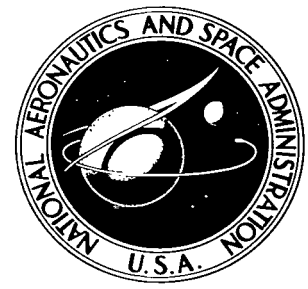

DETECTION OF FLOW-FIELD INSTABILITY IN THE PRESENCE OF BUFFETING BY THE PARTIAL-MODE MODEL TECHNIQUE

by Henry A. Cole, Jr., Robert C. Robinson, and Bruno J. Gambucci

Ames Research Center
Moffett Field, Calif.

NATIONAL AERONAUTICS AND SPACE ADMINISTRATION • WASHINGTON, D. C. • FEBRUARY 1965

DETECTION OF FLOW-FIELD INSTABILITY IN THE PRESENCE OF BUFFETING BY THE PARTIAL-MODE MODEL TECHNIQUE

By Henry A. Cole, Jr., Robert C. Robinson, and Bruno J. Gambucci

Ames Research Center
Moffett Field, Calif.

NATIONAL AERONAUTICS AND SPACE ADMINISTRATION

For sale by the Office of Technical Services, Department of Commerce, Washington, D.C. 20230 -- Price $2.00

DETECTION OF FLOW-FIELD INSTABILITY IN THE PRESENCE OF BUFFETING BY THE PARTIAL-MODE MODEL TECHNIQUE

By Henry A. Cole, Jr., Robert C. Robinson, and Bruno J. Gambucci

Ames Research Center
Moffett Field, Calif.

SUMMARY

The partial-mode model technique for studying buffeting response of launch vehicles is extended to include motion with two node lines in an application to Apollo/Saturn launch vehicles. The results obtained from free-oscillation records are studied through several stages of data refinement including rms, peak values of spectral density, and band width of the spectral density. For the example shown, two unstable flow fields are indicated, one at a subsonic Mach number and another at a supersonic Mach number.

INTRODUCTION

In the prediction of the dynamic response of a rocket launch vehicle to buffeting, it was shown in reference 1 that consideration should be given not only to the buffeting force input but also to the stability of the aerodynamic flow field. Although in principle it is possible to include the flow-field stability effects in buffeting calculations, the uncertainties involved in estimating these effects are large. Consequently, determining the stability of the various separated flow fields on the vehicle is an important part of the buffeting problem.

The stability of a large number of nose configurations has been investigated by the partial-mode model technique described in references 1 and 2 and, from these results, a similarity parameter has been developed (ref. 3) for evaluating aerodynamic stability. Unfortunately, these results are limited to configurations for which the separated flow is confined to the region forward of the first node line. Configurations with more extensive separated flow still require wind-tunnel testing. One such study in which the separated flow extended back to the second node line has been conducted at the Ames Research Center in conjunction with the development of Apollo/Saturn launch vehicles (ref. 4). The purpose of the present report is to describe the extensions in the partial-mode model technique which were made to include motion back to the second node line and to indicate the information which can be obtained through analysis of free-oscillation records.

PARTIAL-MODE MODEL TECHNIQUE

In the partial-mode model technique a single structural mode is selected for study and only the motion of the part of the mode which falls within the separated flow region is simulated. This procedure together with lightweight construction results in a very low generalized mass which amplifies the effect of motion sensitive aerodynamic forces in the area of interest. Consequently, these forces can be measured more accurately with the partial-mode model than with the true scale model. For this reason, the partial-mode technique is particularly useful in detecting the stability of localized separated flow fields and the effects of local geometric changes (refs. 1, 2, and 5).

In the case of the Apollo/Saturn vehicle, the second bending mode was selected for study because it had the lowest product of generalized mass and natural frequency and the buffeting generalized force inputs were estimated to be large in regions of the antinodes. The separated flow area of interest was the nose section forward of the second node line as indicated in figure 1. Since previous applications of the technique included only areas forward of the first node line, the special mechanical device shown in figure 2 was devised to achieve the desired motion. The internal mechanism, consisting of beams connected by flexures, deflects in such a way as to cause the escape rocket tower to rotate in a direction opposite to the main body. The moment arms of the internal beams were selected to place the node line at the desired location. Views of the internal mechanism, the external matching points, and the rear body cross flexures are shown in figures 3, 4, and 5, respectively. The holes on these parts indicate efforts to lighten the generalized mass.

The body shells on the models were made with sandwich construction in order to achieve rigidity and lightness. The inner cylindrical shell was made with three layers of 0.004 glass fiber cloth over the forward half and four layers over the remainder. The filler consisted of donut-shaped sections cut from a 2 lb/cu ft polyurethane foam log. The outer layer consisted of two layers of glass fiber cloth. Polyester resin, used as a bonding agent throughout, was applied sparingly. The tower was built with 3/16-inch diameter aluminum tubing bonded with an epoxy resin containing an aluminum filler. On assembly, the model mounting rings were bonded to the inner cylindrical shell with 828 epoxy resin.

During the course of the wind-tunnel tests, the tower configuration on the full-scale vehicle was changed, which is the reason for the difference between the transonic and supersonic models. The completed transonic model which was 66 inches long weighed 7.63 pounds and the supersonic model which was 68 inches long weighed 8.5 pounds. This included all components attached to the body before installation on the internal mechanism. The weight of the moving internal mechanisms was 1.96 pounds. The completed transonic model is shown mounted in the Ames 14-Foot Transonic Wind Tunnel in figure 6.

TEST EQUIPMENT

The data from a Mach number of 0.70 to 1.16 were obtained in the Ames 14-Foot Transonic Wind Tunnel, at Reynolds numbers from 3.8×10^6 to 4.3×10^6. The data from a Mach number of 1.5 to 2.5 were obtained in the Ames 9- by 7-Foot Supersonic Wind Tunnel at Reynolds numbers between 2.1×10^6 and 2.4×10^6. Both wind tunnels have sting-type model supports mounted on struts which span the tunnels aft of the test sections.

The models were instrumented with strain-gage bridges mounted on the resonant spring shown in figure 3. These gages were powered by 20 kc carrier current amplifiers. Direct current components were eliminated from demodulated data signals by high pass filters before being recorded on magnetic tape. The attenuation due to filtering was negligible above 10 cycles per second. To calibrate the strain gages, filters were bypassed, static loads were imposed on the model, and the deflections were measured with dial gages while the strain-gage output was read from a digital voltmeter. Before each wind-tunnel test, an ac reference signal of known voltage and frequency was recorded.

The frequency response of the model, mounted in the wind tunnel, was obtained by driving the model at discrete frequencies with an electromagnetic shaker. Input to the shaker was sinusoidal. Figure 7 shows the setup for measuring wind-off frequency response. The force input to the model was obtained from the force gage and the model response from a strain-gage bridge mounted on the resonant spring. Amplitude ratio and phase angle of the input and output signals were computed by a frequency response analyzer which has tracking filters (at the input) that pass only a narrow band of frequencies centered at the driving frequency.

Analysis of the recorded data consisted of measurement of the over-all rms, the spectral density, and the statistical distribution of amplitude for each record. The rms of deflection and moment was obtained by applying the static calibration factors to the rms voltage as read from a true rms meter. Spectral analysis was done with a heterodyne type analyzer in which an oscillator swept through the frequency range. The band width of the filter used in the analysis was 1.7 cycles per second.

The statistical analysis was done on a hybrid digital-analog computer. Reference 6 describes this equipment and its operation.

MEASURED RESPONSE

To determine the aerodynamic flow effects, the dynamic characteristics of the model were measured with the wind off and on. With wind off, the model was driven by an electrodynamic shaker as shown in figure 7, and with wind on, by the buffeting forces. This section will describe the various measurements

which were made and interpret the results through several stages of data analysis, the rms, spectral density, spectral density peaks, and, finally, band width of the model-mode spectral peak.

Wind Off

Static and dynamic deflection measurements for the two models are shown in figures 8 and 9. The articulating motion of the internal mechanism is evident on the static deflection measurements. At zero frequency, there is considerable sting deflection, but at the model design frequency the impedance of the sting reduces the deflection to negligible values and the nodal point on the model is at the desired location.

Frequency responses of the two models are shown in figures 10 and 11 where M_i and M_o are the input and output moments. The values have been corrected for inertia of the attachment fittings. The theoretical single-degree-of-freedom curve is shown on the figures for comparison. Deviations from this curve are caused by extraneous modes, some of which are identified in the figures. However, it may be seen that the principal peak occurs at the model mode frequency and, hence, the experiment is well conditioned.

Wind On

The primary purpose of the tests was to determine the effect of flow-field instability on the buffeting of the launch vehicle. A washer was placed at the base of the escape rocket to alter the flow field. Configurations with and without the washer are shown in figures 6 and 7, respectively. The response was measured with each configuration in both subsonic and supersonic flow. Some typical time histories of strain-gage output (measured on resonant spring) are shown in figures 12 and 13, which, it may be noted, vary from responses containing many frequencies to responses containing predominantly the model frequency.

Root mean square.- The time histories were reduced to rms form to give an over-all picture of the response which could be used to indicate the conditions where more refined analysis might prove fruitful. The rms measurement included the effects of extraneous modes as well as the mode of interest and, hence, can only be used for qualitative purposes.

The root mean square of the pitching-moment coefficient with and without the washer is plotted in figure 14 versus Mach number at zero angle of attack ($\alpha = 0^\circ$). The following definition was used:

$$C_m = \frac{\theta_m K}{qSd}$$

where

θ_m angular displacement at base of model

K model spring constant

q dynamic pressure

S area of model base

d diameter of model base, 14 in.

It may be seen that the washer causes a considerable rise in the response both subsonically and supersonically. Furthermore, the coefficients show a rising trend at supersonic Mach numbers.

Since for a launch trajectory the dynamic pressure decreases above a Mach number of about 1.5, the angular motion of the model was calculated for dynamic pressures corresponding to the dynamic pressure of a typical trajectory. The results are shown in figure 15 for several angles of attack. The drop off in dynamic pressure tends to compensate for the rise in the pitching-moment coefficient and the curves are relatively flat in the supersonic region. Again it may be seen that the washer caused a considerable rise in response for all conditions.

Examination of figure 15 reveals an important point. As angle of attack is increased, the response increases at subsonic Mach numbers whereas it decreases at supersonic Mach numbers. This effect could be caused by either a reversal in trend of the buffeting input or the aerodynamic damping. Since the rms does not distinguish between these two effects, it is necessary to refer to spectral densities for further information.

Spectral densities.- The spectral density shows the frequency distribution of the mean-square value of the time history and, hence, is useful for obtaining quantitative results concerning the generalized buffeting input and aerodynamic damping of the mode of interest. Since spectral density information is much more difficult to obtain than the rms, the qualitative results obtained from the rms study were used to select the time histories on which spectral analyses were made.

Some of the spectral densities calculated for the two models are shown in figure 16. Although it is intended that the partial-mode model restrict motion to a single degree of freedom, other modes are always present. When the response of the extraneous modes becomes large relative to the mode of interest, the results become questionable because of possible nonlinearities in the aerodynamic forces. One such condition is shown in figure 16(a). The large peak which occurs near 30 cps is associated with the sting first-bending mode. The rise in $C_{m_{rms}}$ in figure 14 at 0.8 Mach number is due to response of this mode. In figure 16(b), the sharp peak near 44 cps for the washer-on configuration was due to a violent shaking of the tower at a Mach number of 1.16 which only occurred at this one condition. For all other

subsonic test conditions, the predominant response was in the desired mode. Several examples of spectral densities measured with the supersonic model are shown in figures 16(c) through (f). It may be noted that the dominant peak occurs in the mode of interest near 94 cps.

Since the height of the spectral peak at the frequency of mode of interest indicates the combined effect of aerodynamic damping and generalized force input, a study was made of the peak values as shown in figures 17 and 18. In figure 17, the effect of angle of attack with and without the washer is shown for several subsonic and supersonic Mach numbers. Subsonically, the spectral density peaks tend to be lowest at 0° angle of attack and rise as angle of attack is increased. The point for washer on at $M = 0.80$ and 2° angle of attack shows an exceptionally high rise indicating the possibility of unstable aerodynamic damping. Supersonically, the highest spectral density peaks occur near 0° angle of attack. Since the possibility of unstable aerodynamic damping near 0° angle of attack is indicated for three points, the variation with Mach number was investigated as shown in figure 18. The large effect of the washer on the mode of interest at supersonic Mach numbers is apparent here. The rising trend of the washer-on value near a Mach number of 1.5 is particularly interesting since this is near maximum dynamic pressure in the launch trajectory.

As mentioned before, the height of the spectral density peak is determined by the generalized buffeting force input as well as the aerodynamic damping. The band width, on the other hand, is determined mainly by the aerodynamic damping. Hence, a study of the band widths of the mode of interest was made at points where spectral peaks indicated possible unstable aerodynamic conditions. Figure 19 shows the amplitude spectral density at $M = 1.51$ at 0° angle of attack. The band width was measured at an amplitude of 0.707 of the peak amplitude. The value of 2.25 cps is less than the wind-off value of 3.5 cps in figure 11 and, hence, indicates unstable aerodynamic damping. The curve for 4° angle of attack is also shown on the figure for comparison, and it may be seen that the increase in angle of attack stabilizes the aerodynamic damping. It may also be noted that the frequency of the peak value varies in a manner that suggests a nonlinear pitching moment curve similar to the one reported in reference 1.

Similar studies of band width were conducted for other conditions and results are given in the following table:

Subsonic model				Supersonic model			
Mach number	Angle of attack	Band width		Mach number	Angle of attack	Band width	
		Washer off	Washer on			Washer off	Washer on
0	---	3.5 - 4	3.5 - 4	0	---	3.5 - 4	3.5 - 4
.8	0	4 - 6	5 - 7	1.5	0	4 - 7	2 - 2-1/2[a]
.8	2	4 - 6	1.5 - 3.5[a]	1.5	2	4 - 7	6 - 10
.8	4	---	3.5 - 5.5	1.5	4	5 - 10	6 - 8
1.16	0	5 - 7	7 - 8	2.5	0	3 - 5	3 - 4.5
1.16	2	5 - 7	12 - 15	2.5	2	4 - 6	4 - 7
				2.5	4	5.5 - 8	5 - 10

[a]Unstable aerodynamic damping indicated.

It may be seen from the table that unstable aerodynamic damping is also indicated for the washer-on configuration at $M = 0.8$, $\alpha = 2^{\circ}$. At $M = 2.5$, $\alpha = 0^{\circ}$, both the washer-off and washer-on configurations appear to be near neutral stability. The range of values in the table reflects uncertainties in the measurements.

Probability distributions.- In order to provide information on absolute values which occurred during the buffeting tests, a study was made of the distribution of points on the time histories (ref. 6). Equal samples were taken from each condition. The results shown in figure 20 indicate that the data follow the normal distribution up to about three times the rms and then fall below. On the basis of results from reference 1, the peak values would be expected to follow the Rayleigh distribution and similarly drop off above three times the rms.

CONCLUSIONS

From subsonic and supersonic wind-tunnel tests of a partial-mode model in which motion was represented back to the second node line, it has been determined that significant measurements of motion-sensitive aerodynamic forces can be made. The principal response in most cases was in the mode of interest and effects of local configuration changes were discernible as follows:

1. Placing a washer at the base of the escape rocket causes an unstable aerodynamic flow field near a Mach number of 1.5 at 0° angle of attack and also near a Mach number of 0.8 at 2° angle of attack.

2. The experimental points follow a normal probability distribution up to three times the rms and then fall below at higher values.

Ames Research Center
National Aeronautics and Space Administration
Moffett Field, Calif., Nov. 25, 1964

REFERENCES

1. Cole, Henry A., Jr.: Dynamic Response of Hammerhead Launch Vehicles to Transonic Buffeting. NASA TN D-1982, 1963.

2. Robinson, Robert C.: A Wind-Tunnel Investigation of the Dynamic Stability of Axisymmetric Models With Hammerhead Noses in Transonic Flow. NASA TM X-787, 1963.

3. Buffeting During Launch and Exit. NASA Space Vehicle Design Criteria. NASA SP-8001, 1964.

4. Aeroelastic and Acoustic Conference, Manned Spacecraft Center. NASA, Office of Advanced Research and Technology, March 6, 1963.

5. Rainey, A. Gerald: Progress on the Launch-Vehicle Buffeting Problem. AIAA Publ. CP-8, Fifth Annual AIAA Structures and Materials Conference, April 1-3, 1964.

6. Cameron, William D.: Hybrid Computer Techniques for Determining Probability Distributions. Presented at the International Symposium on Analogue and Digital Techniques Applied to Aeronautics (Liege, Belguim), Sept. 9-12, 1963.

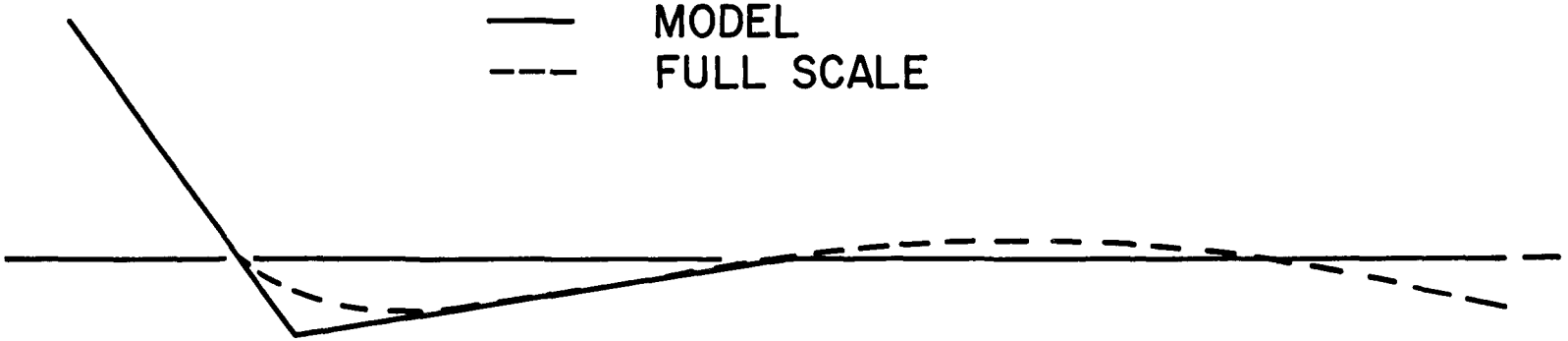

Figure 1.- Approximation of the second bending mode.

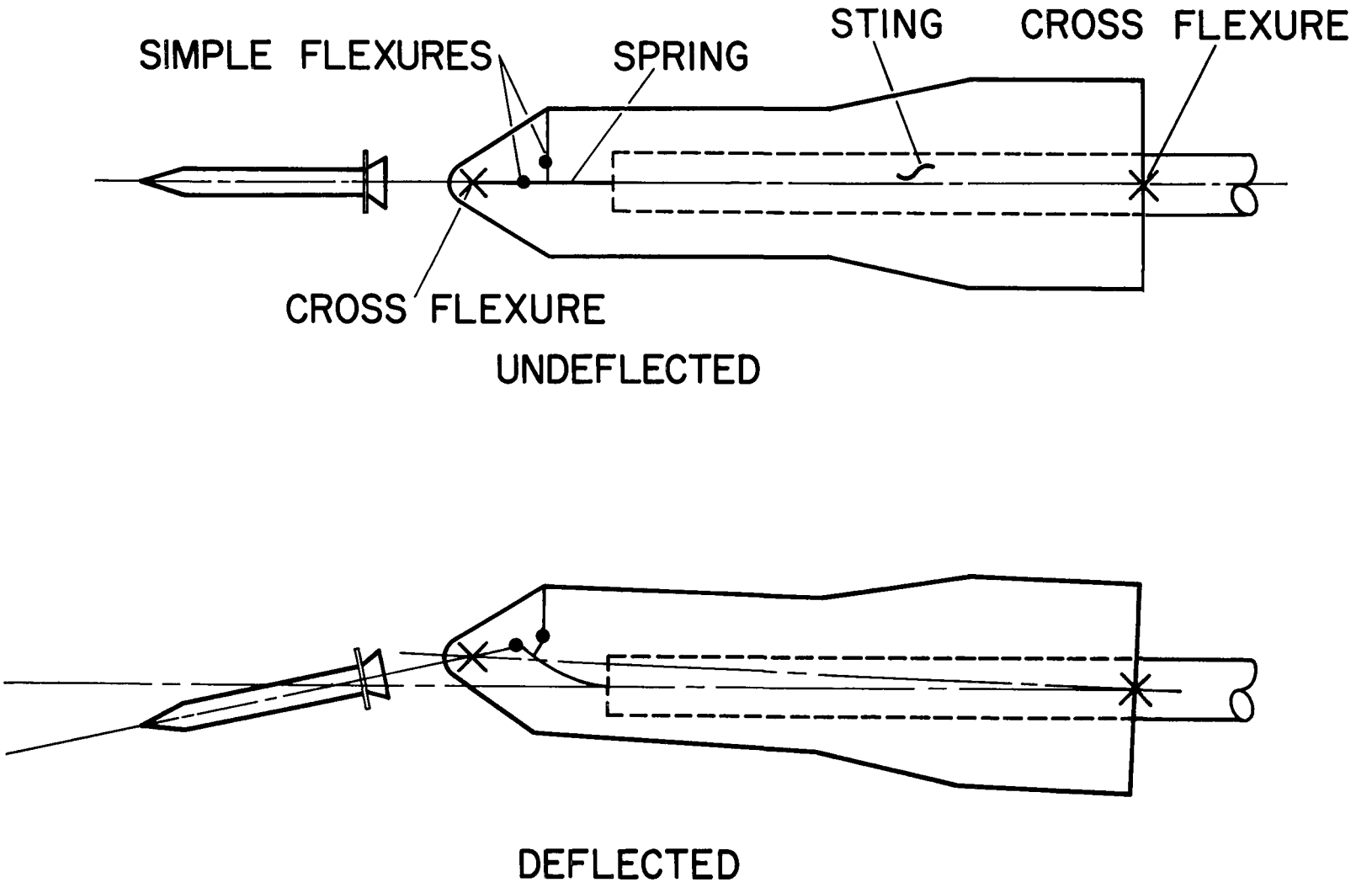

Figure 2.- Schematic drawing of the model.

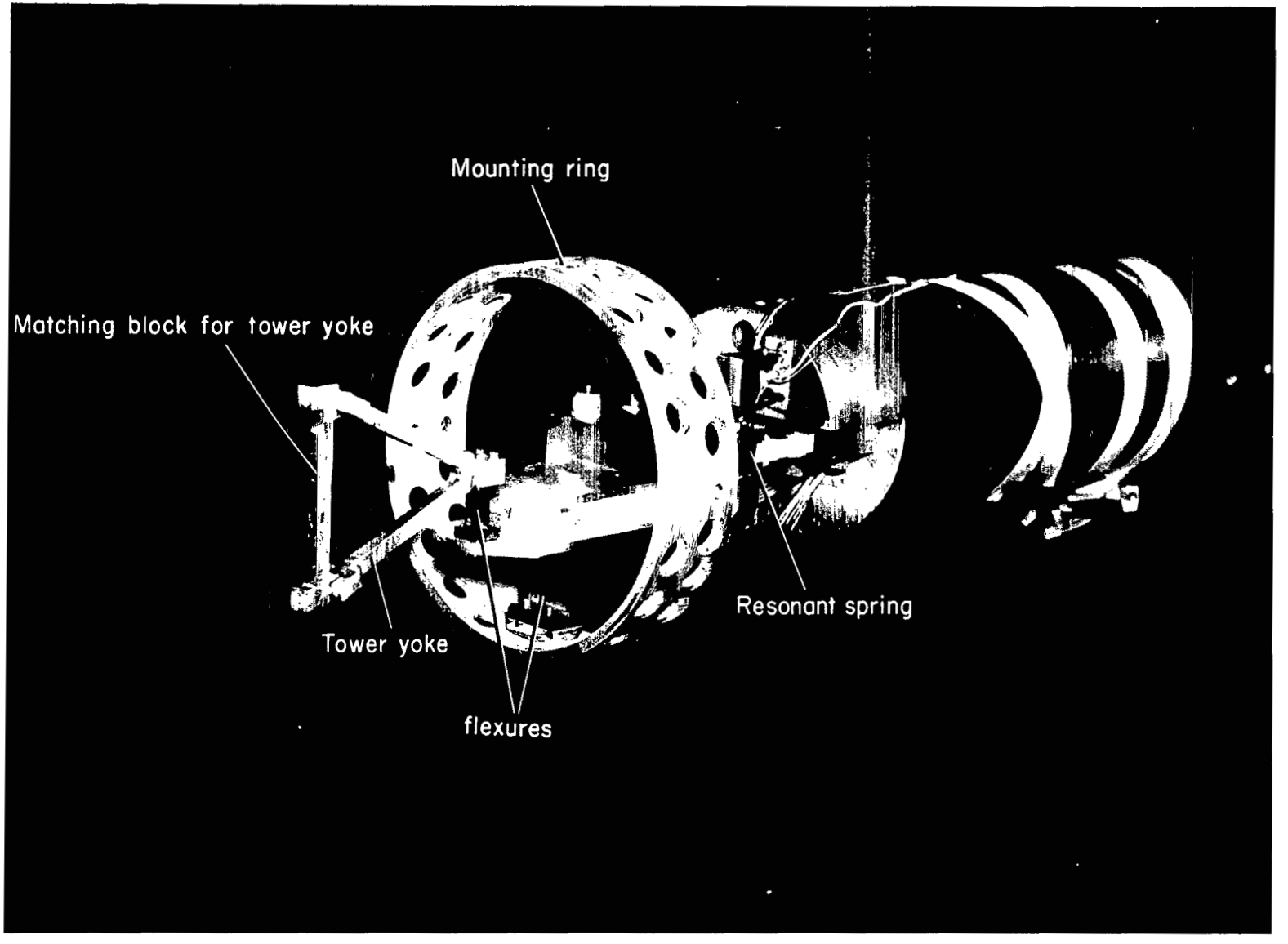

Figure 3.- View of internal mechanism.

A-29457.1

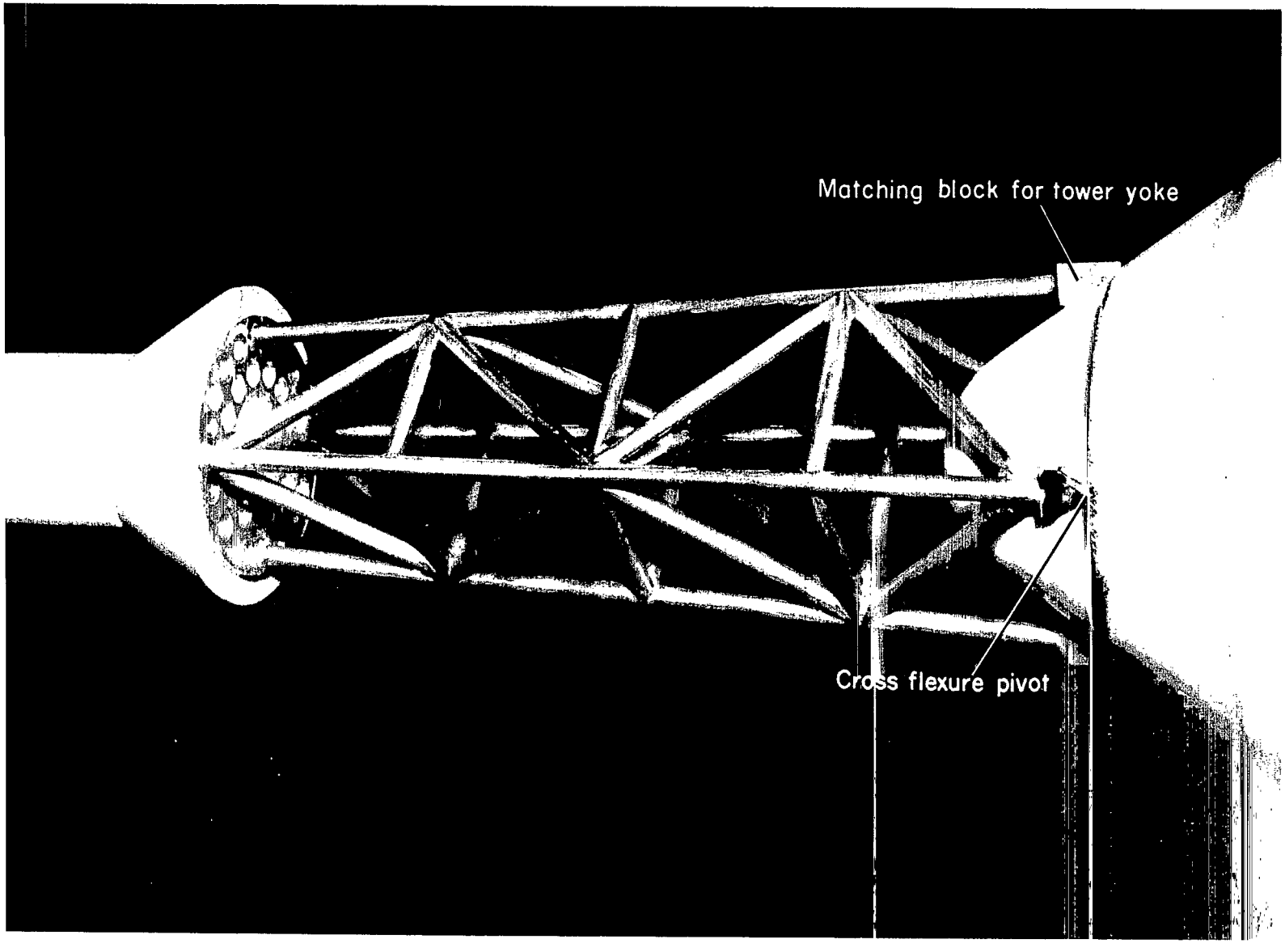

Figure 4.- View of tower.

A-29459.1

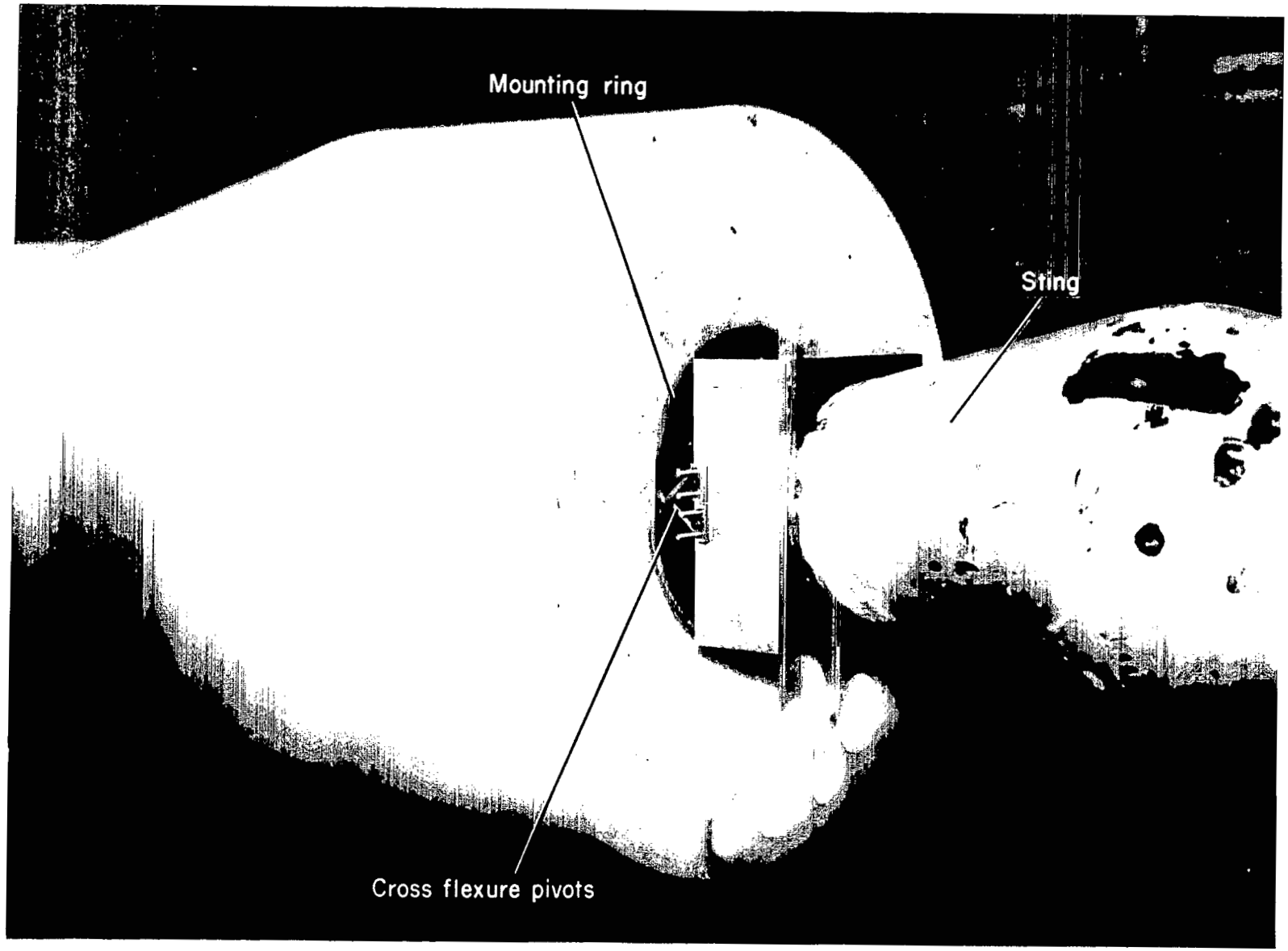

A-28460.1

Figure 5.- View of rear flexures.

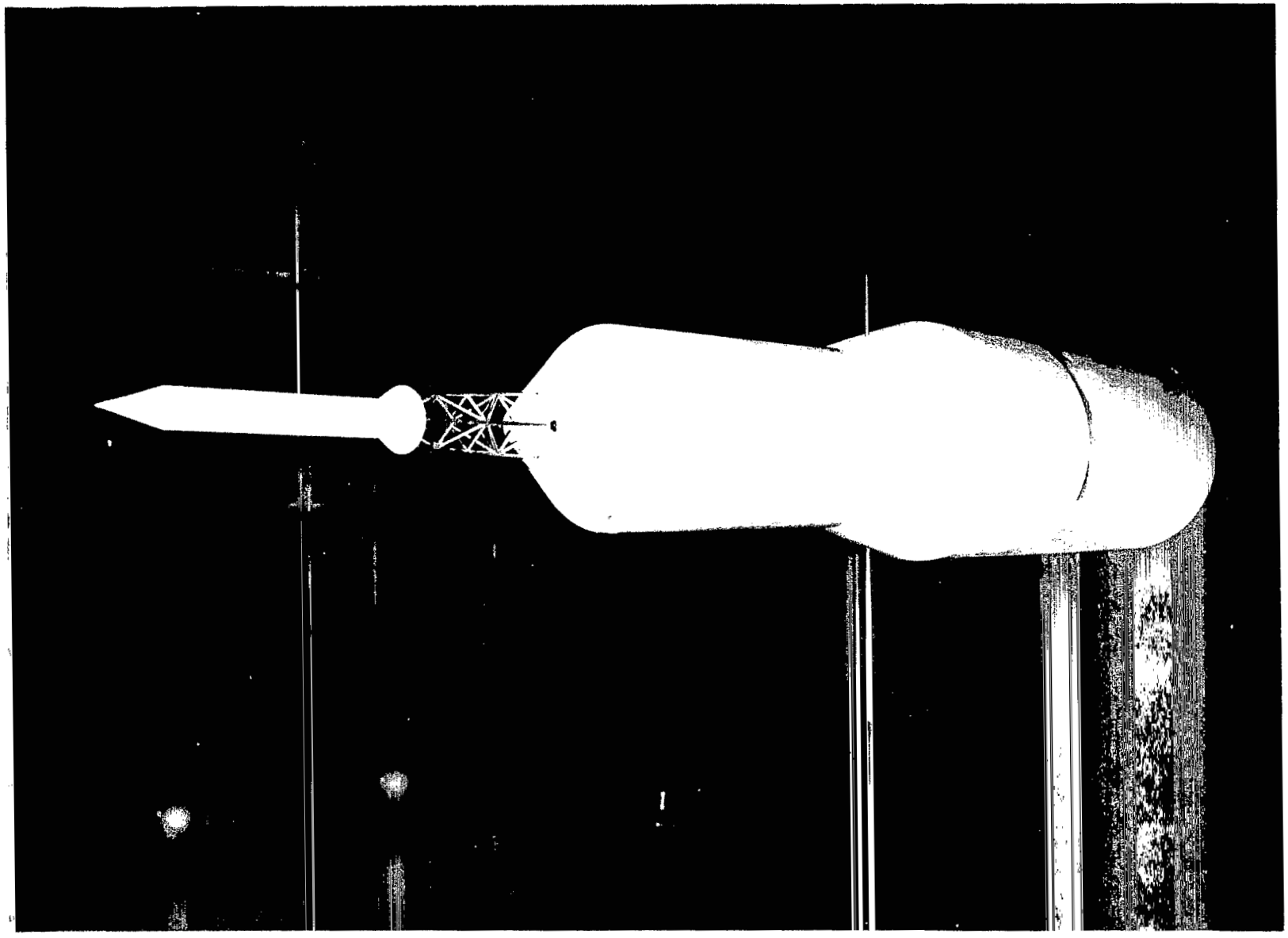

A-29458

Figure 6.- Transonic model mounted in Ames 14-Foot Transonic Wind Tunnel.

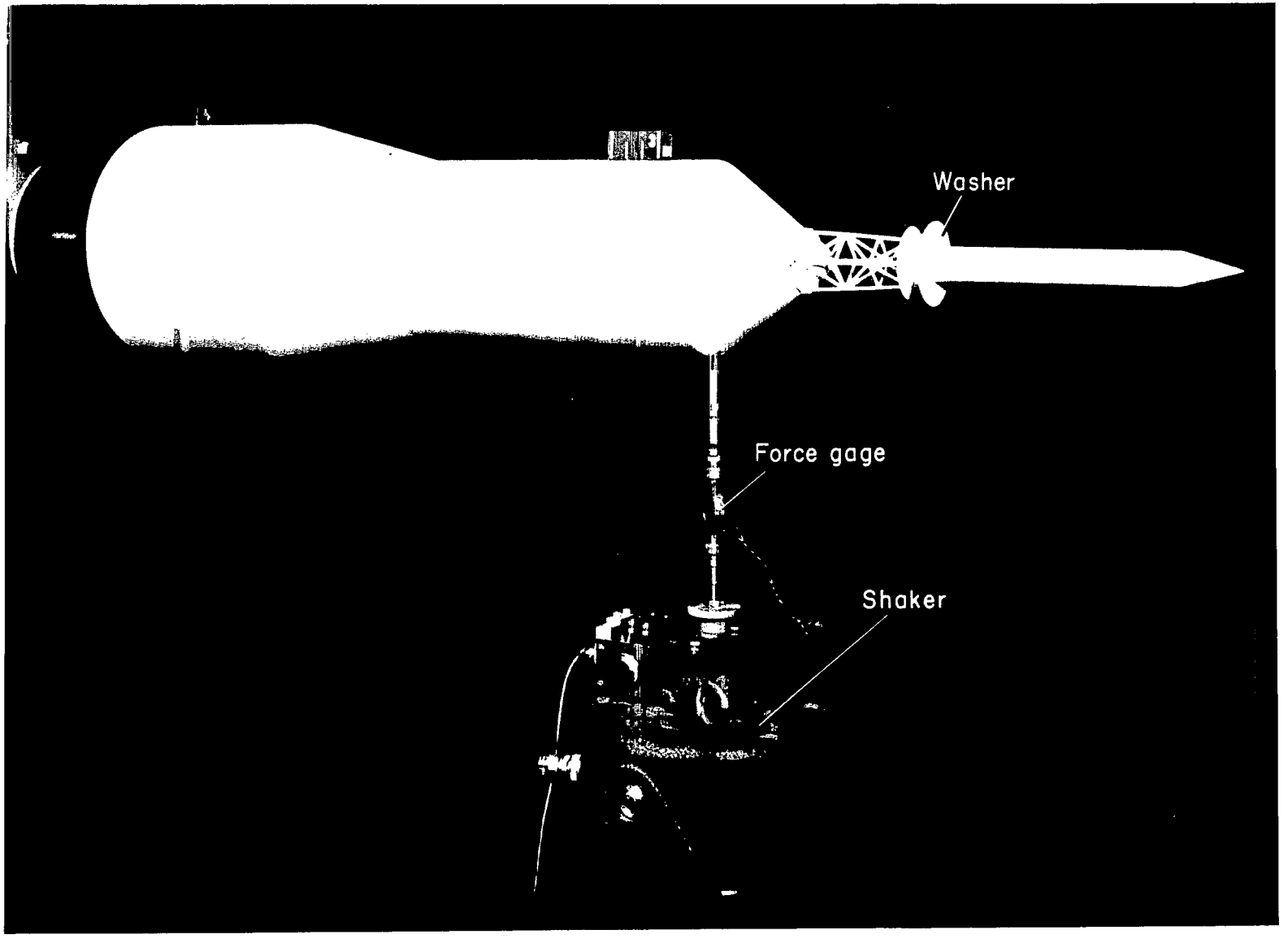

Figure 7.- Shaker installation used in wind-off frequency response tests.

A-32326.1

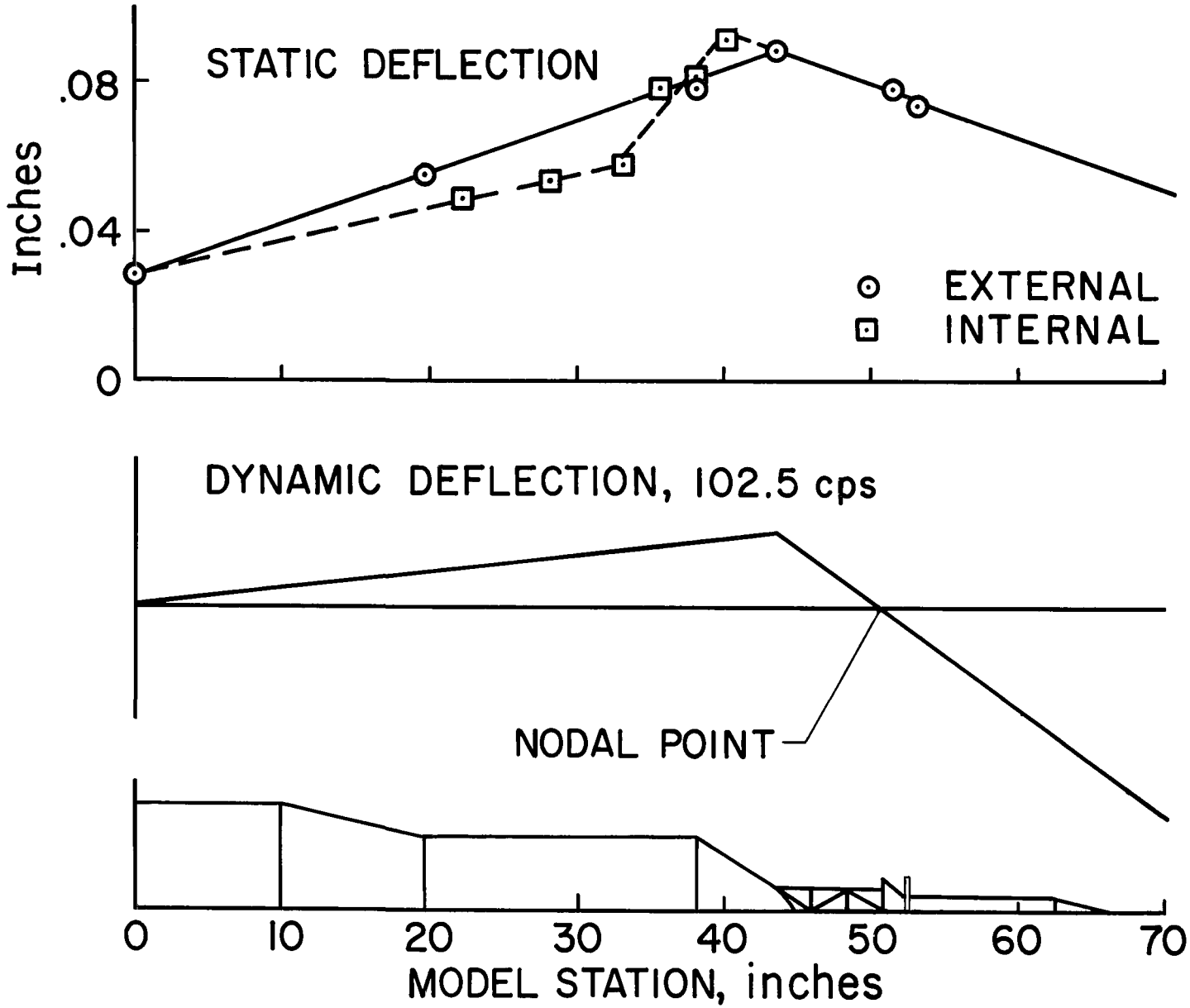

Figure 8.- Measured deflections on transonic model.

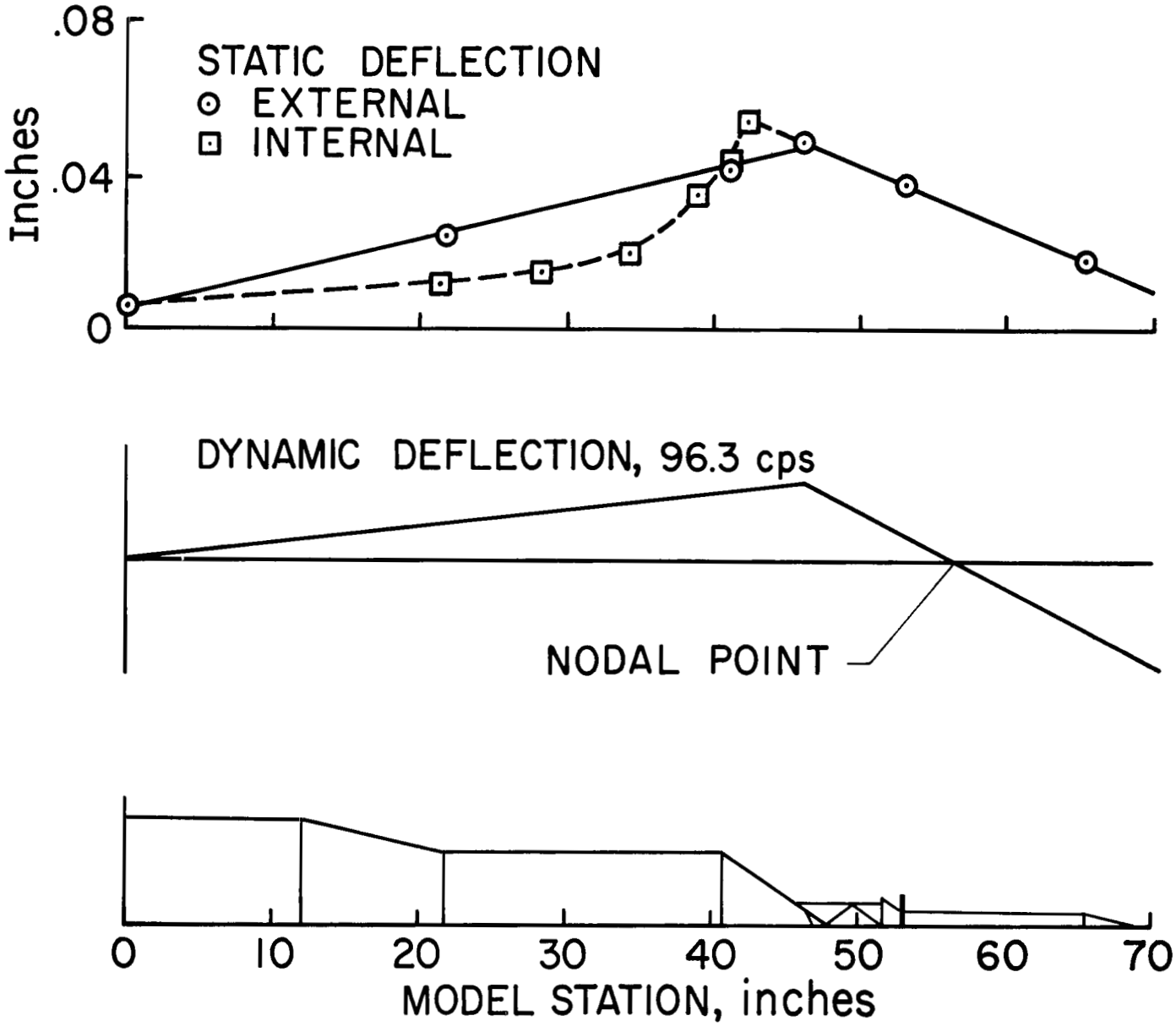

Figure 9.- Measured deflections on supersonic model.

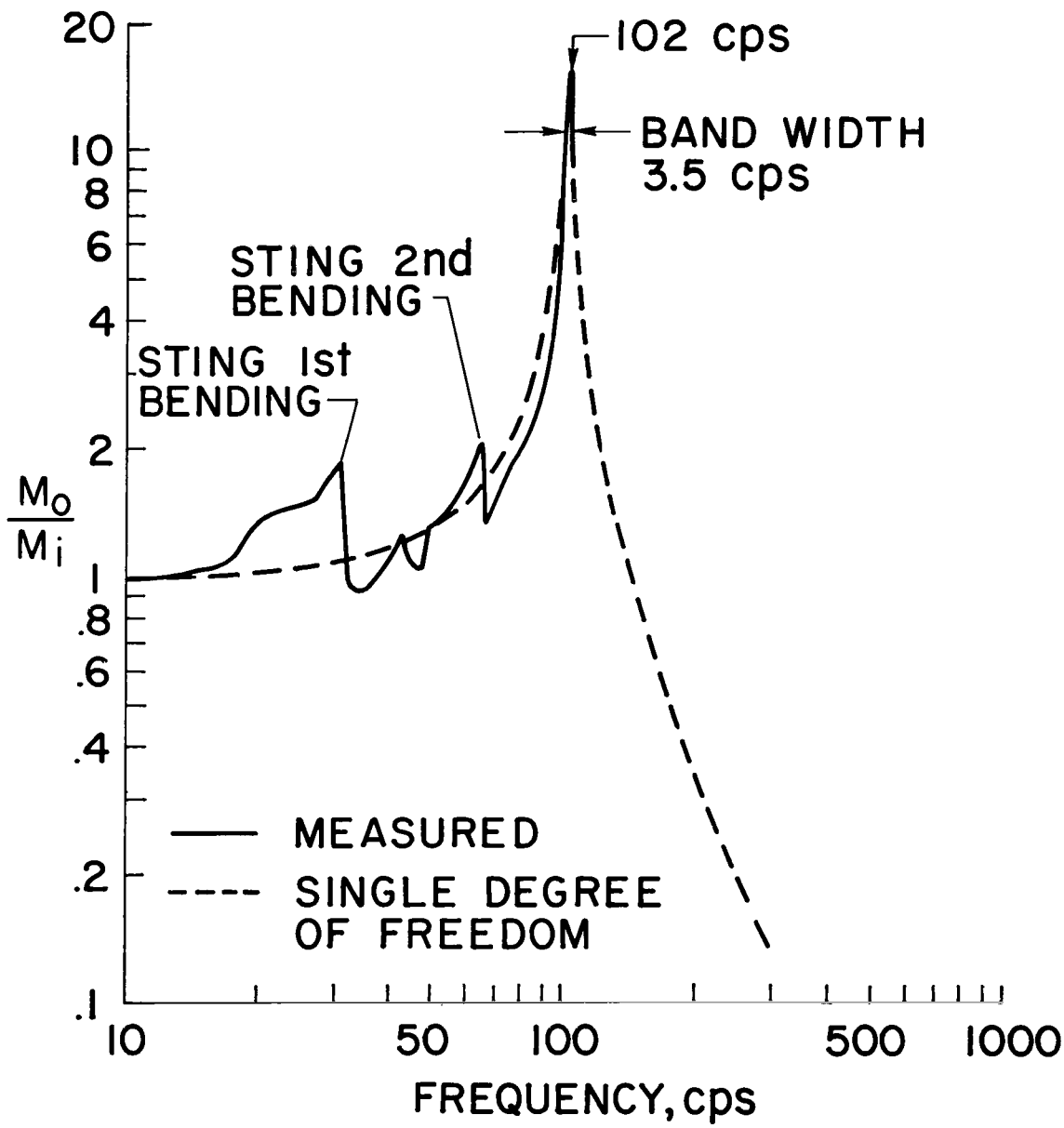

Figure 10.- Frequency response of transonic model.

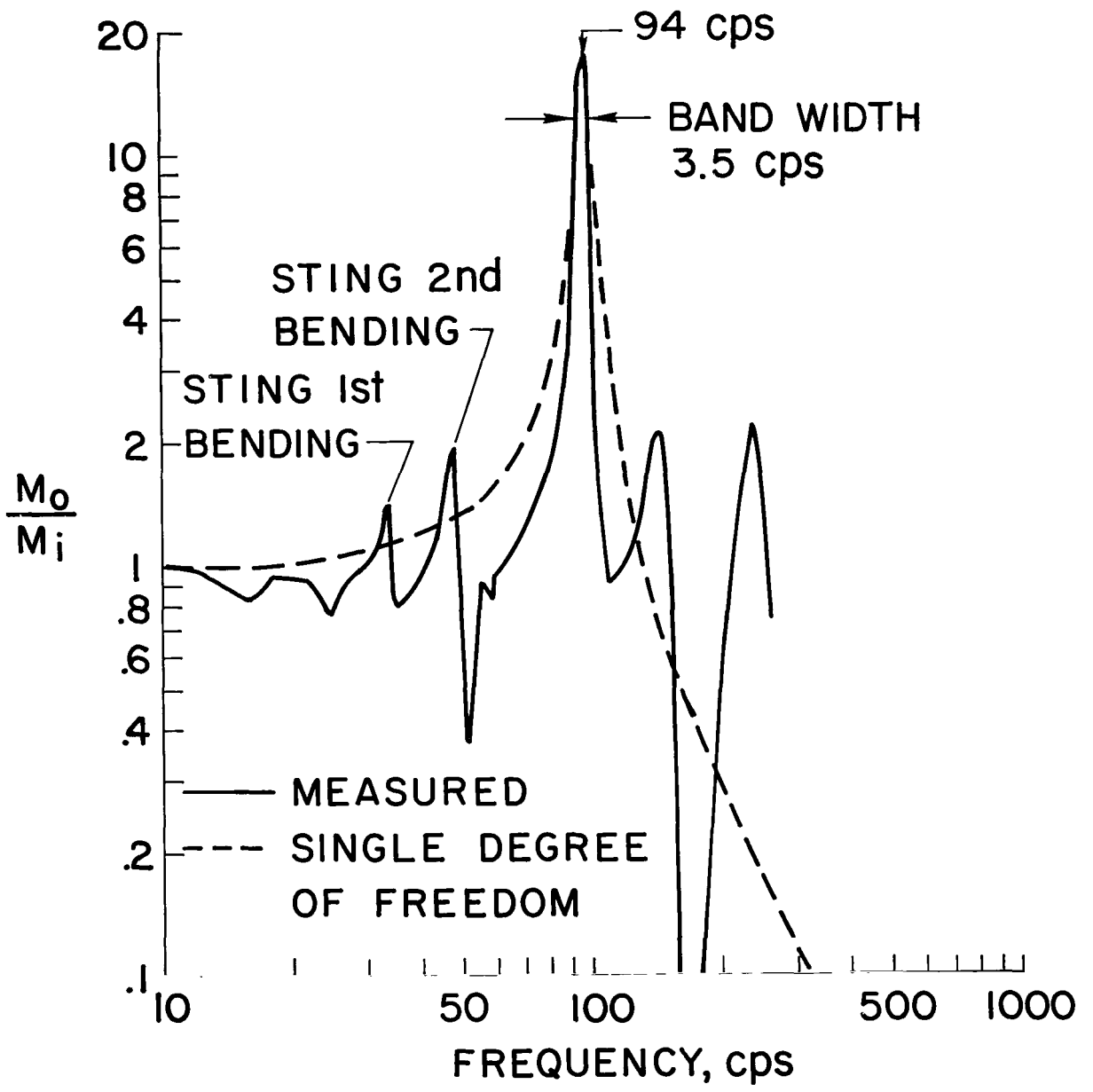

Figure 11.- Frequency response of supersonic model.

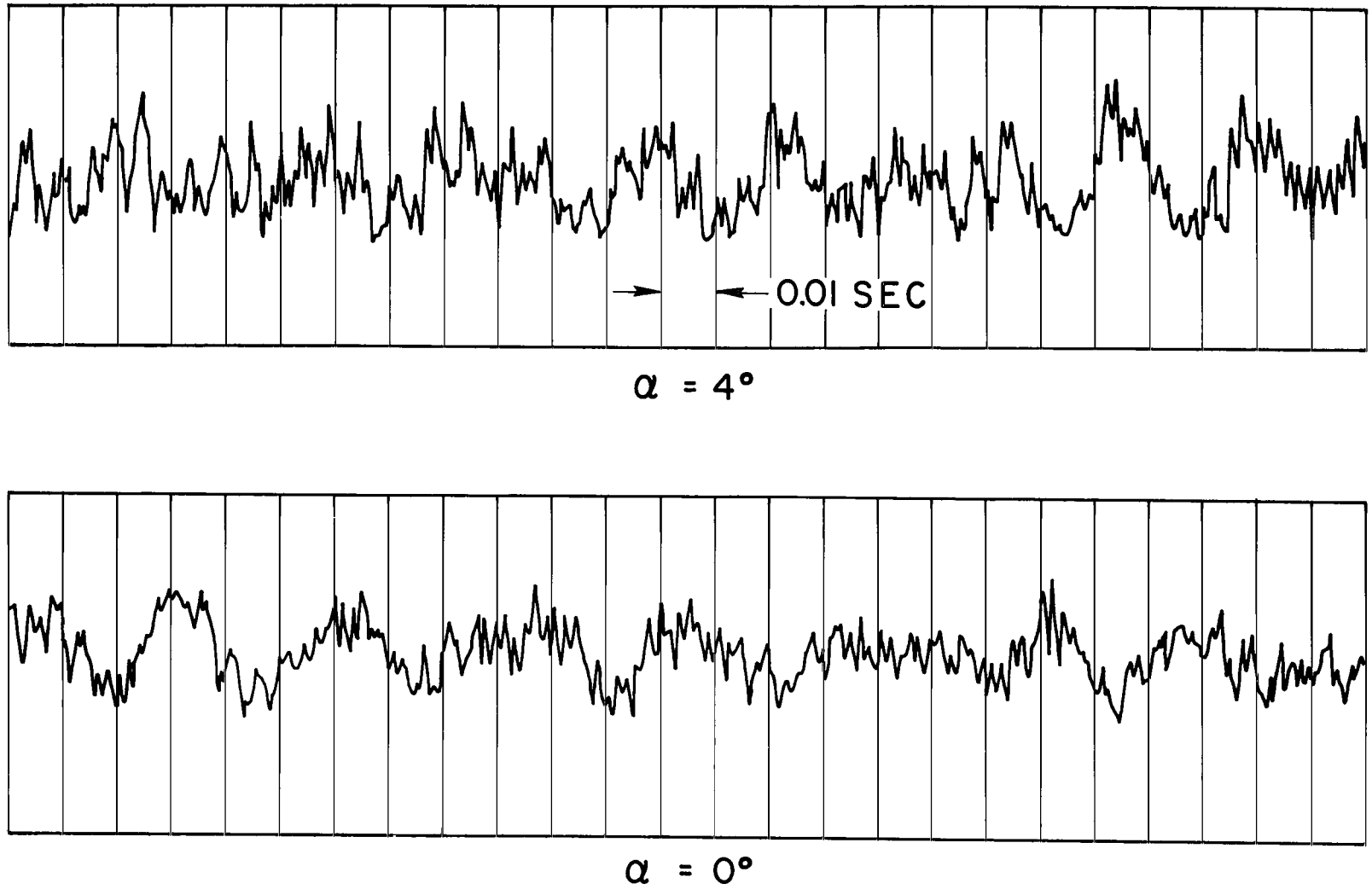

Figure 12.- Sample time histories at a Mach number of 0.80.

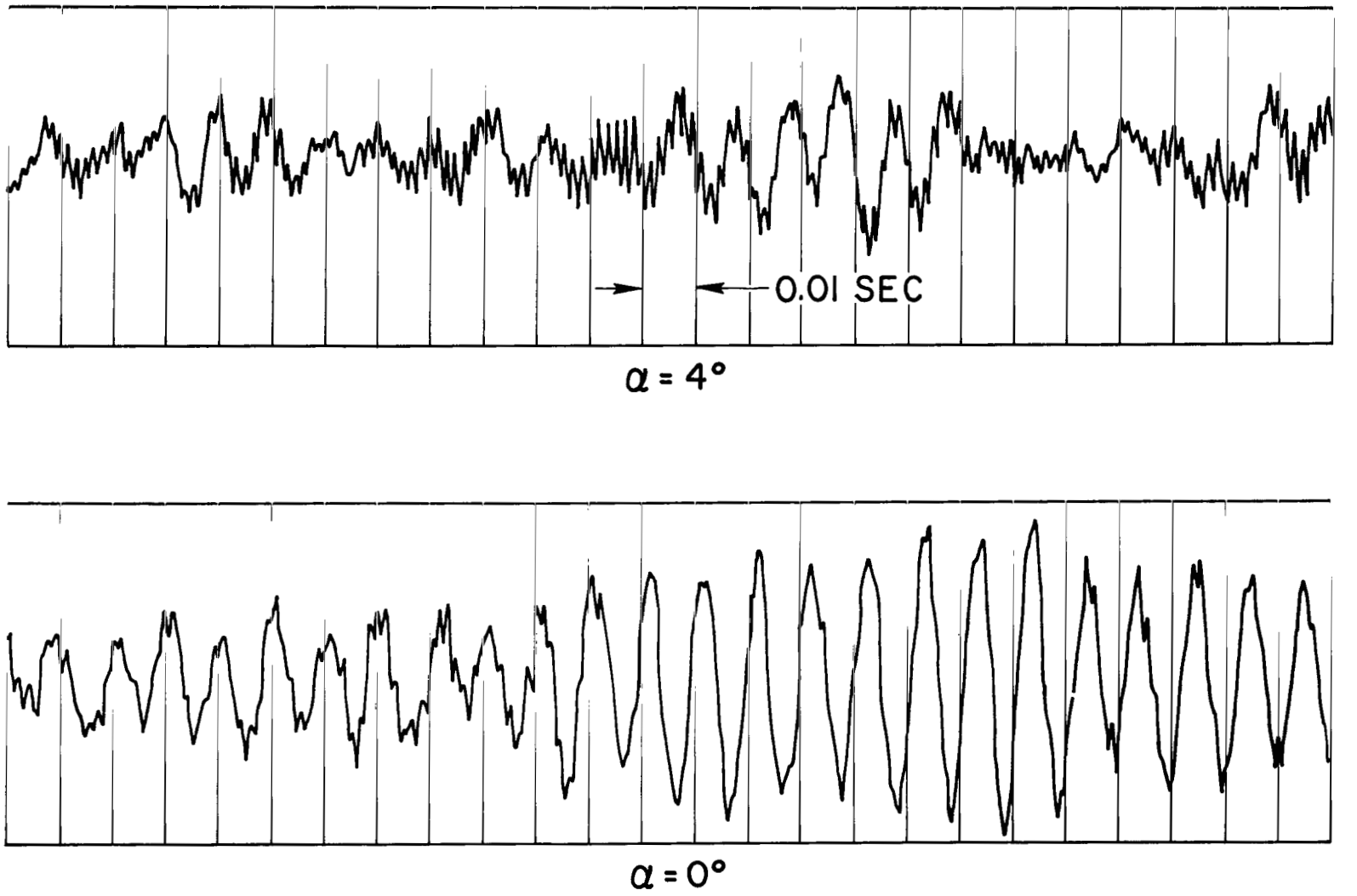

Figure 13.- Sample time histories at a Mach number of 2.50.

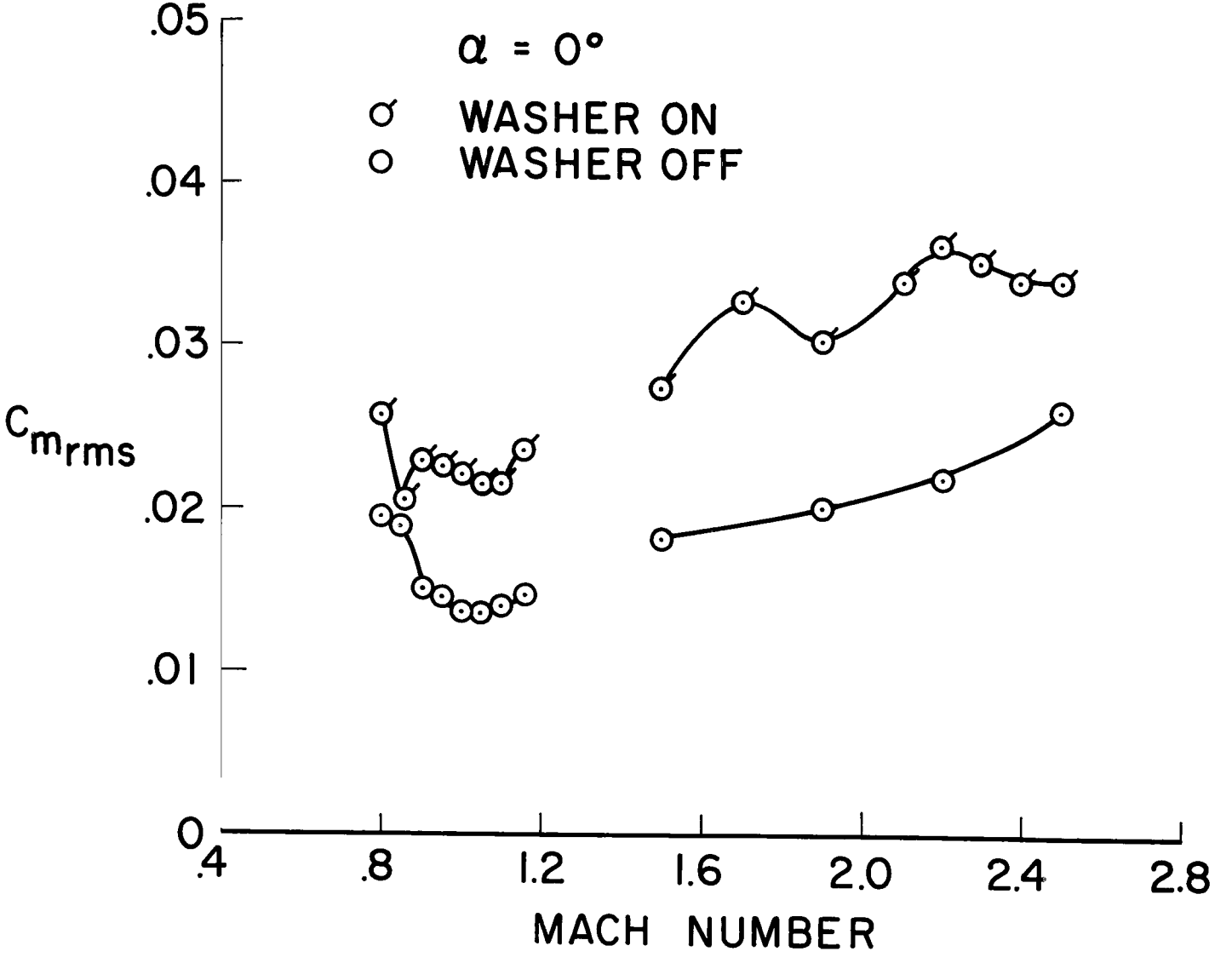

Figure 14.- Variation of pitching-moment coefficient with Mach number at zero angle of attack.

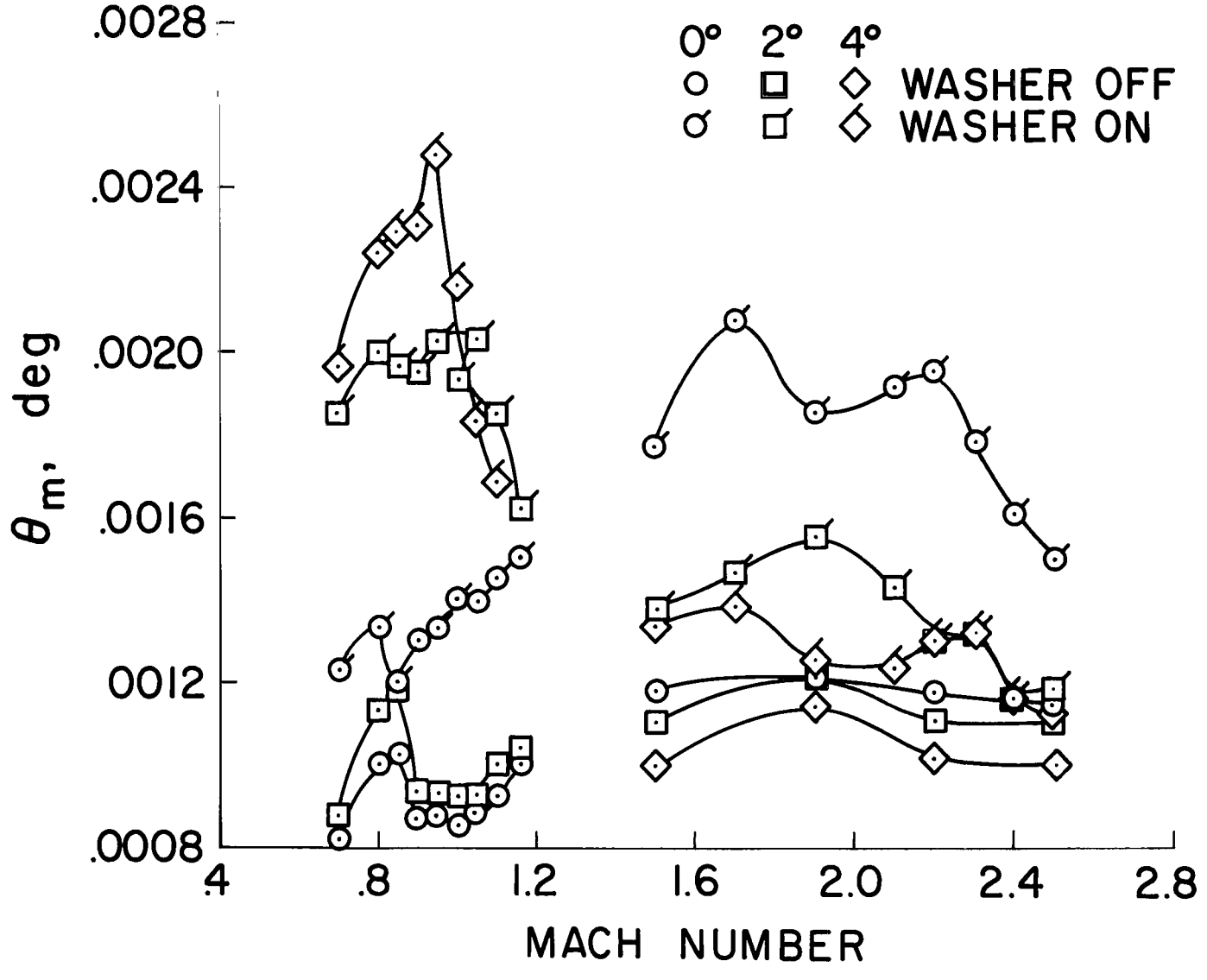

Figure 15.- Root-mean-square angular motion of model base corrected to flight dynamic pressure.

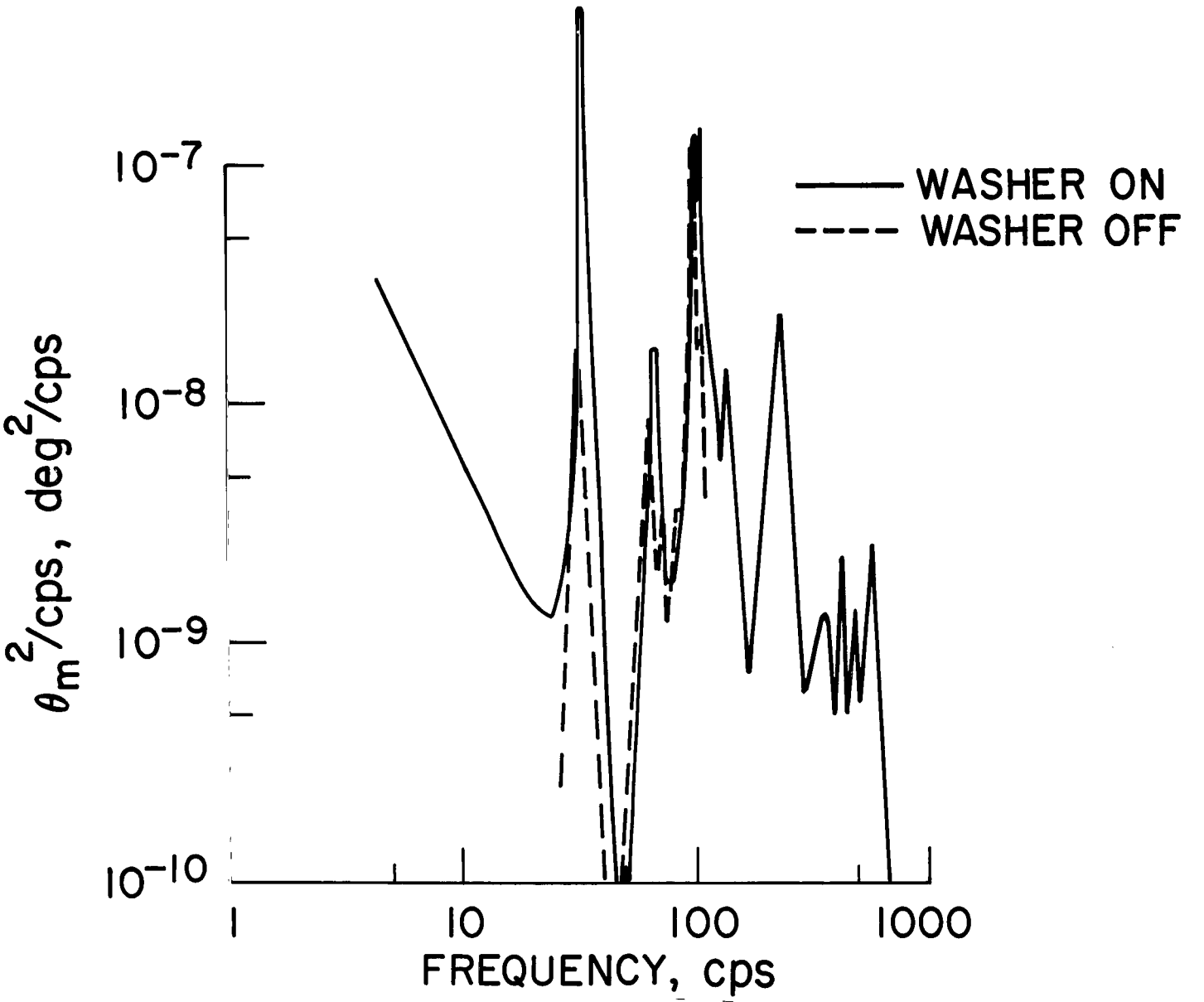

(a) M = 0.80, $\alpha = 0^{\circ}$

Figure 16.- Spectral density at angular motion at base.

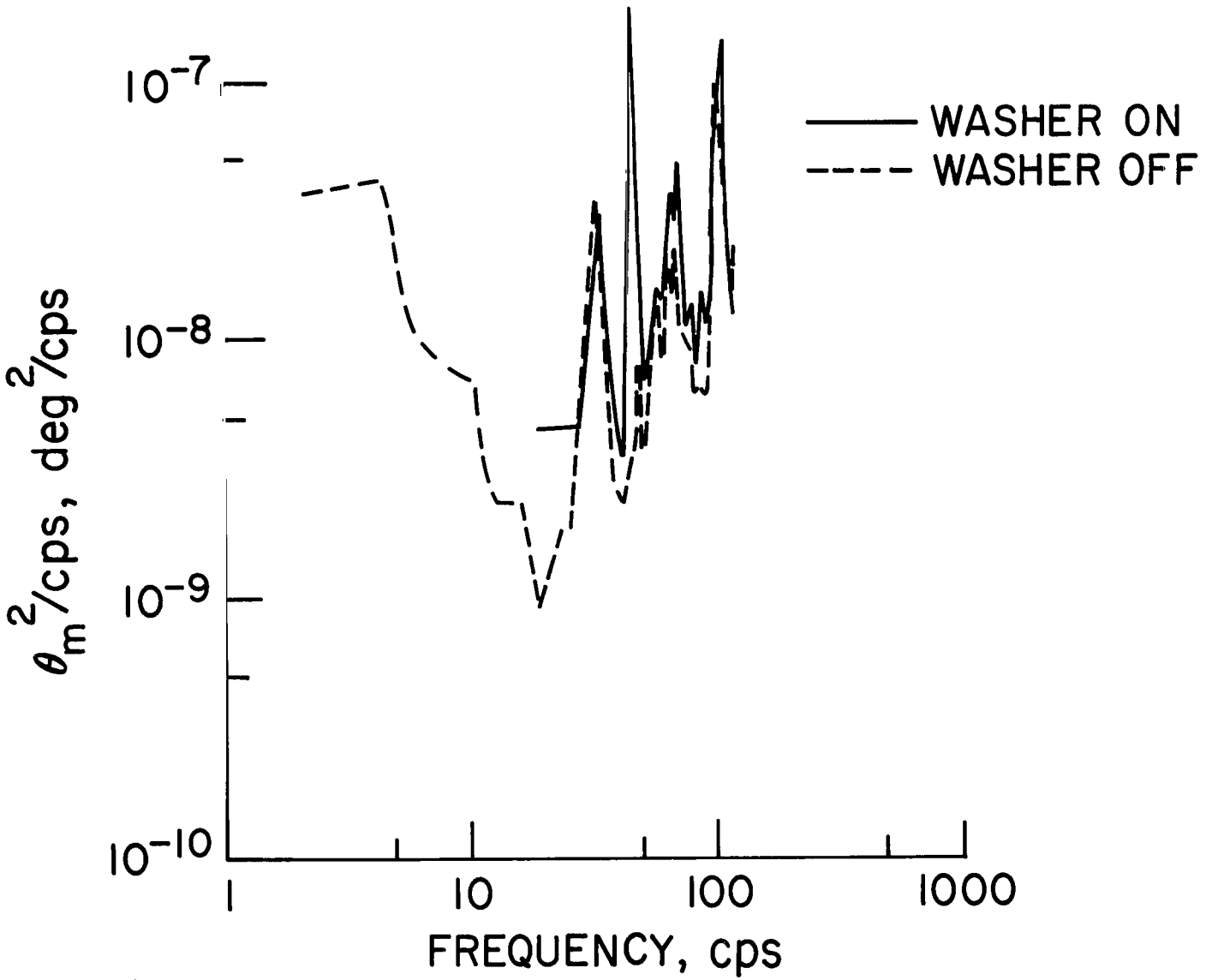

(b) M = 1.16, $\alpha = 0^{\circ}$

Figure 16.- Continued.

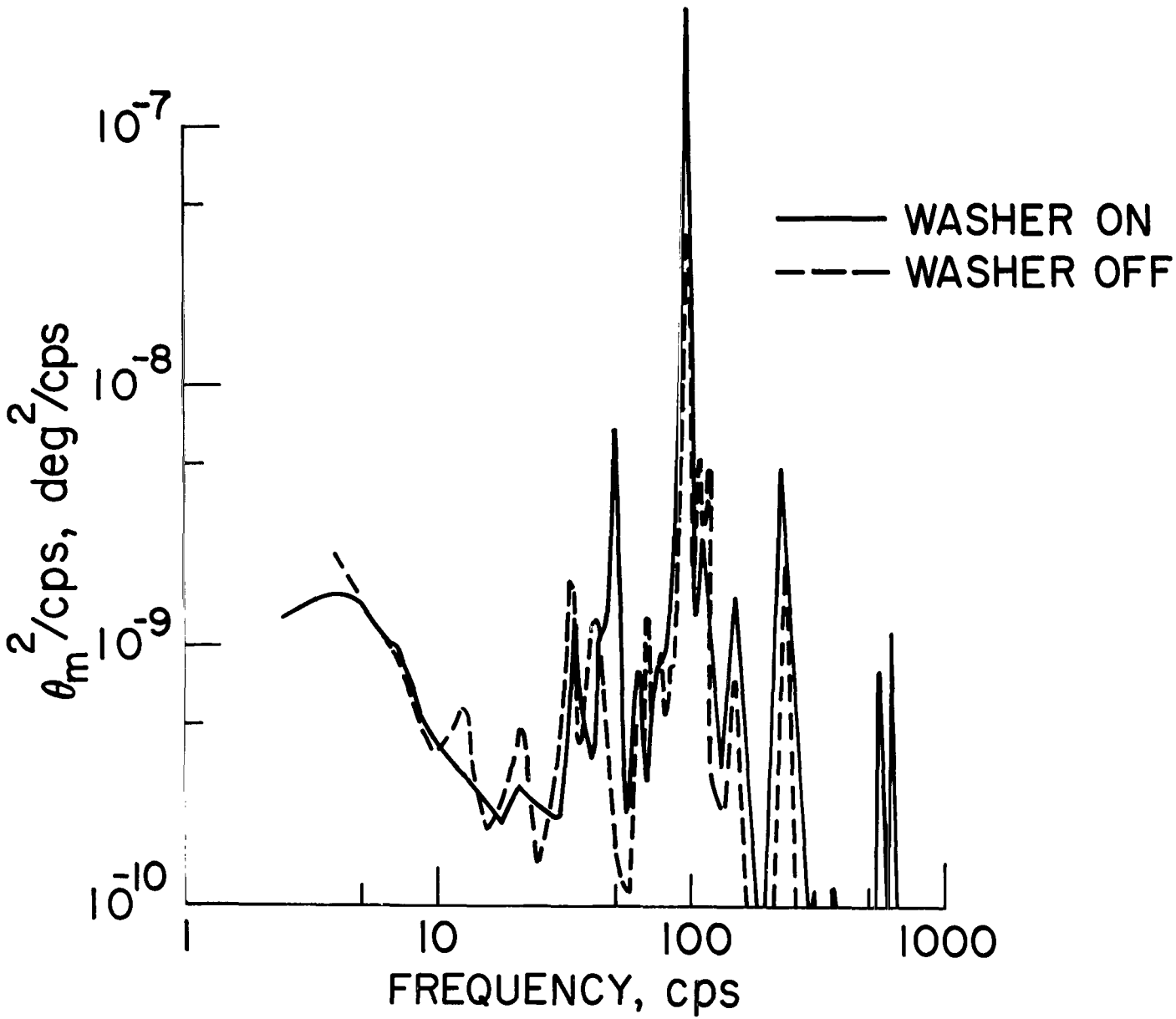

(c) M = 1.50, $\alpha = 0^\circ$

Figure 16.- Continued.

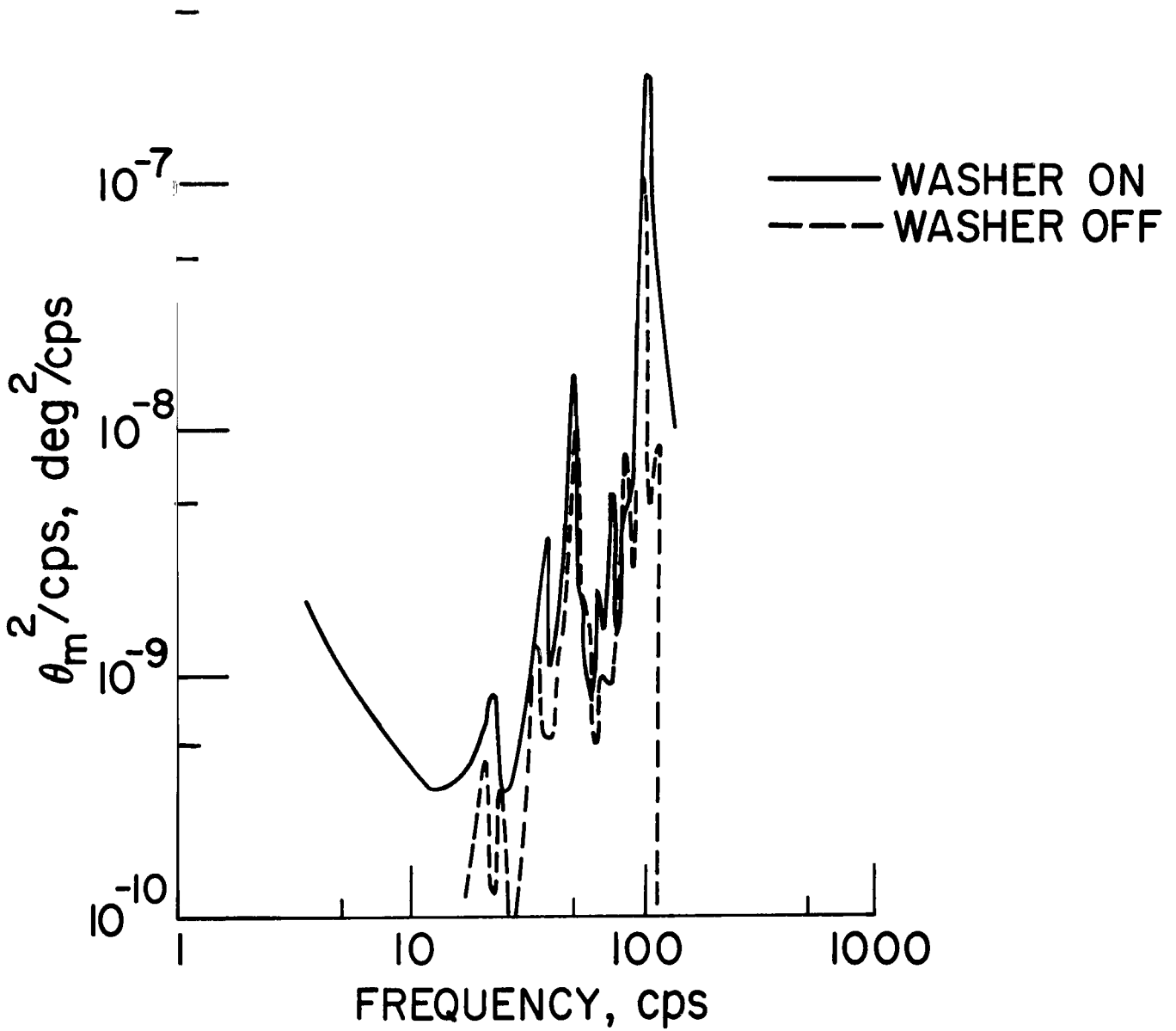

(d) M = 2.20, $\alpha = 0^o$

Figure 16.- Continued.

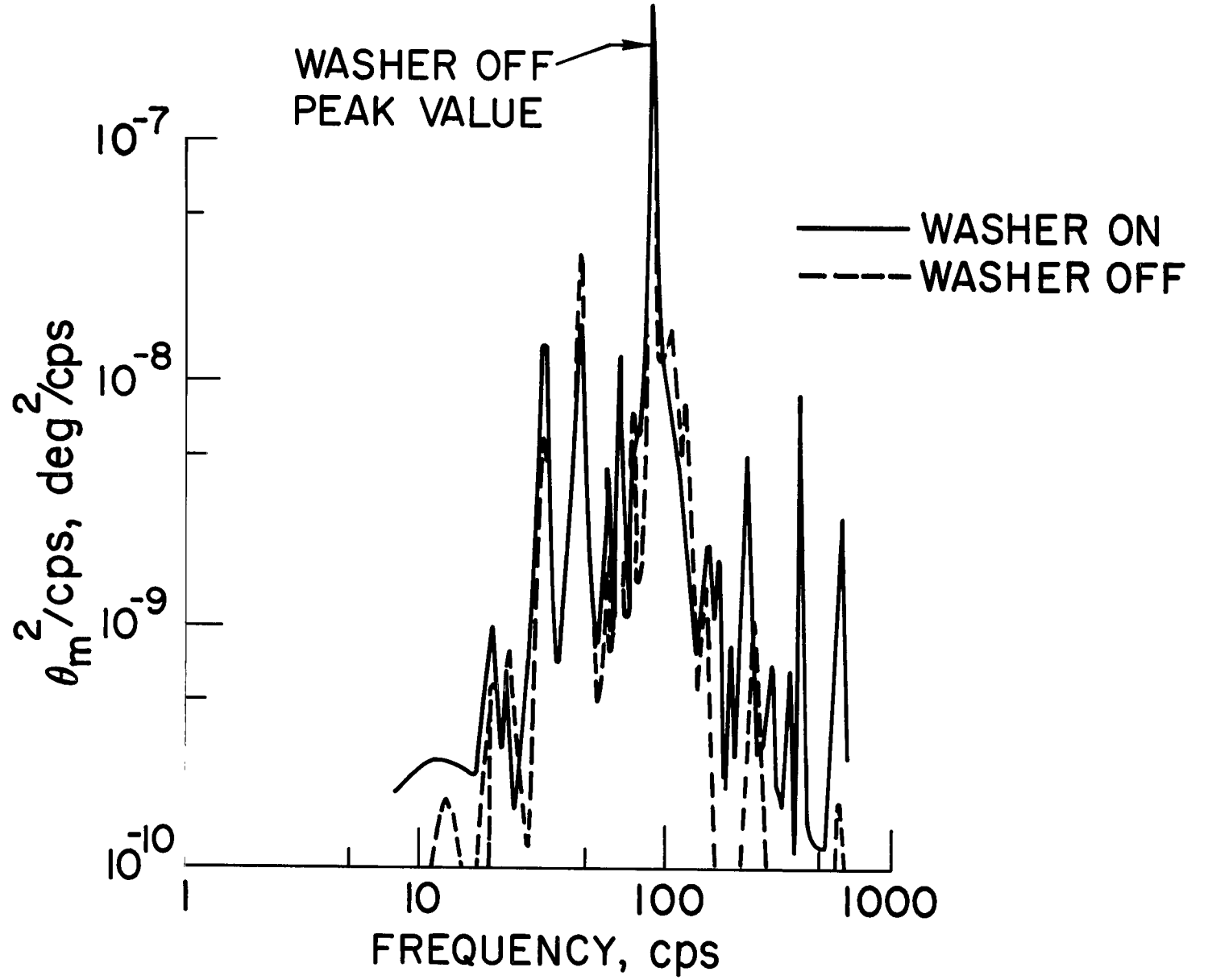

(e) M = 2.50, $\alpha = 0^\circ$

Figure 16.- Continued.

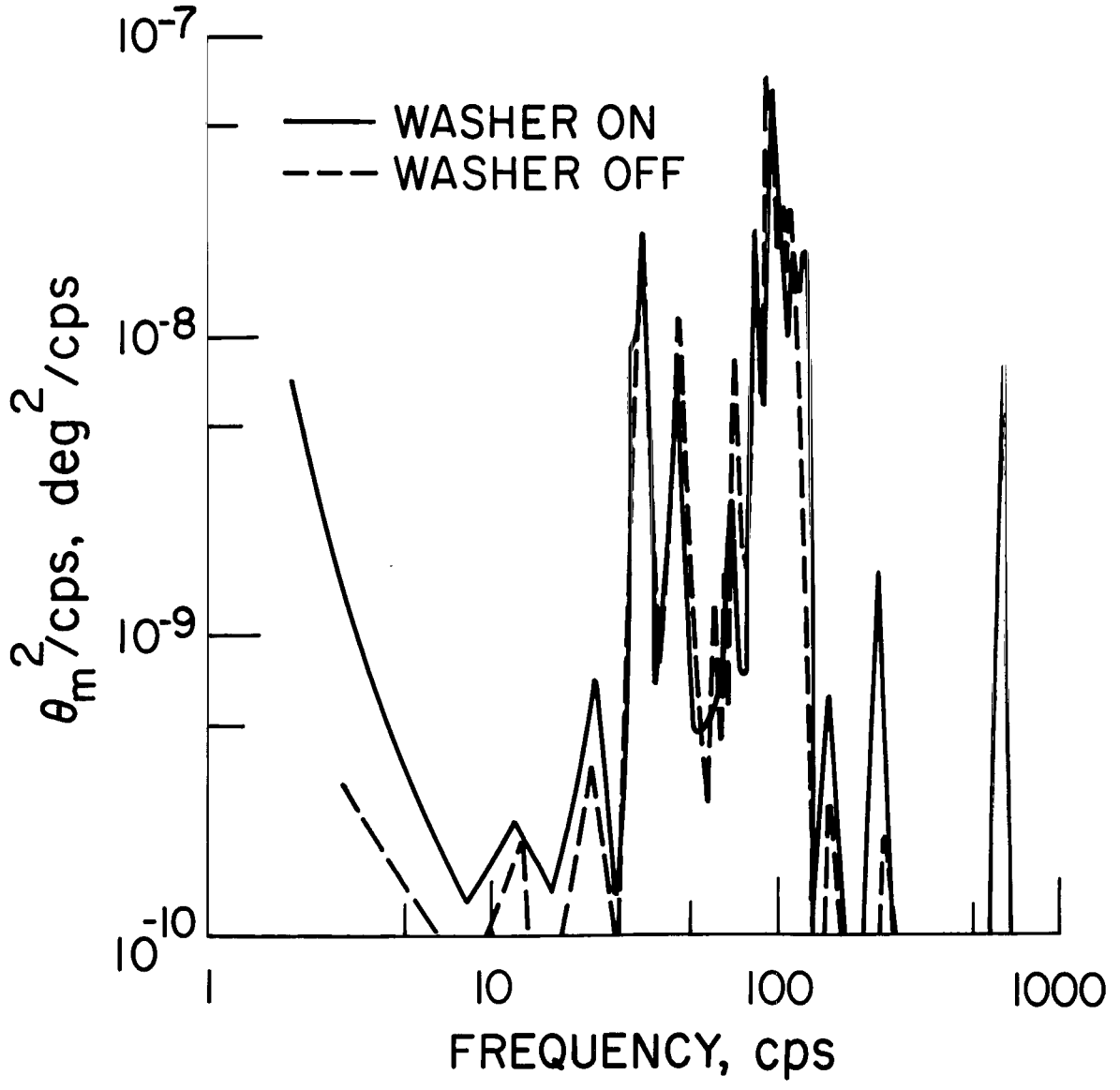

(f) M = 2.50, $\alpha = 4^{\circ}$

Figure 16.- Concluded.

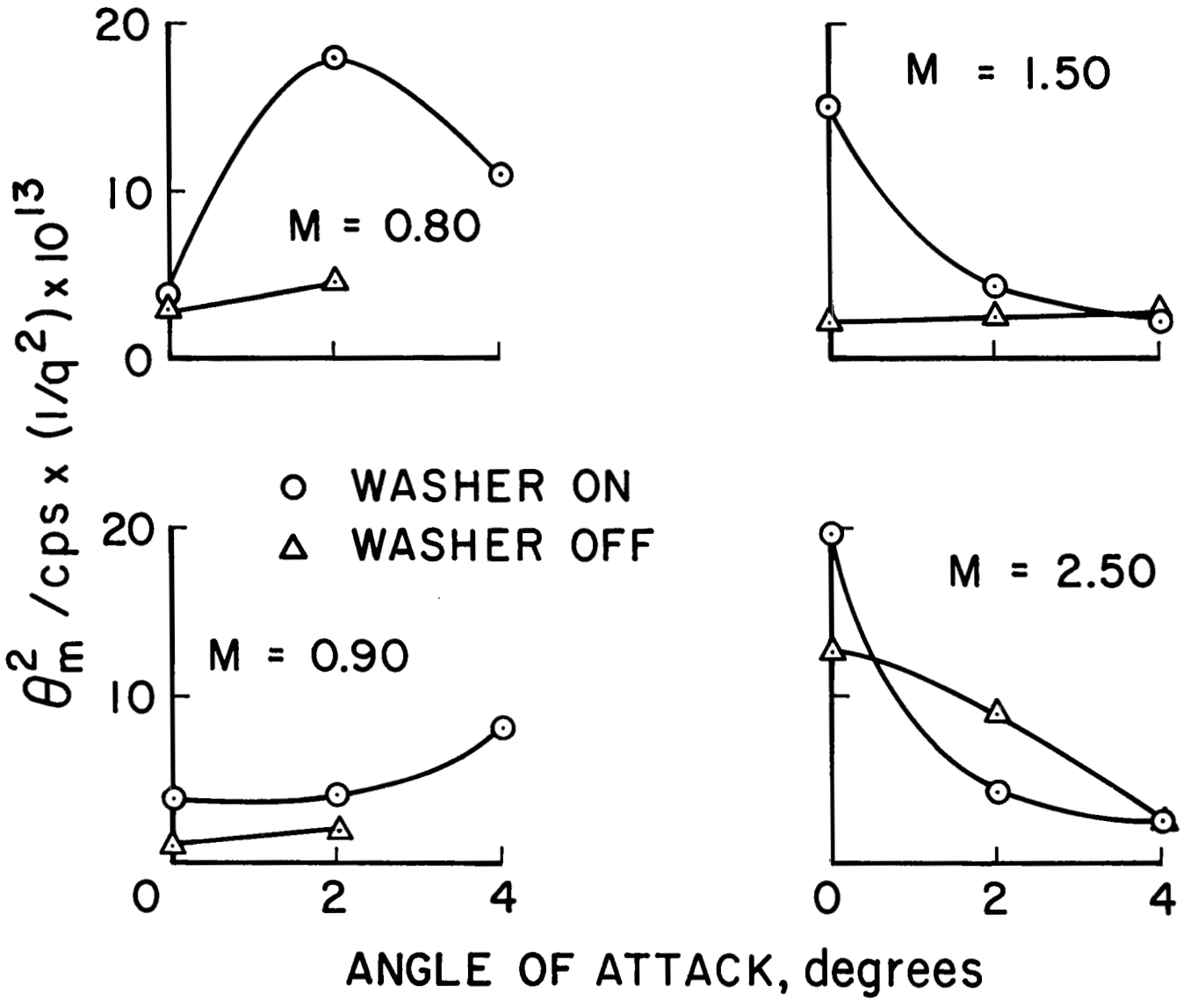

Figure 17.- Spectral density peaks at model resonant frequency.

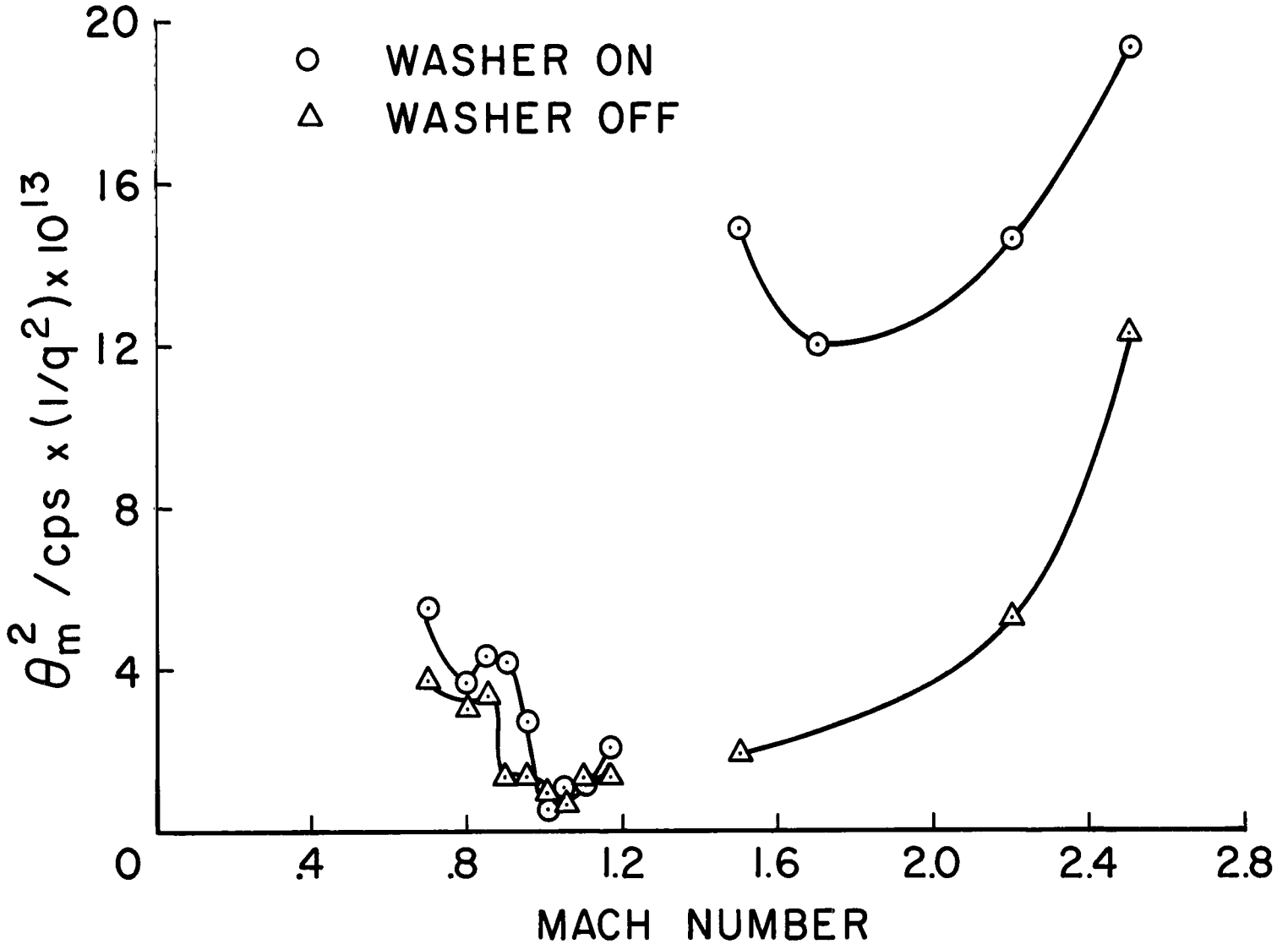

Figure 18.- Variation of spectral density peaks at model resonant frequency for $\alpha = 0^{\circ}$.

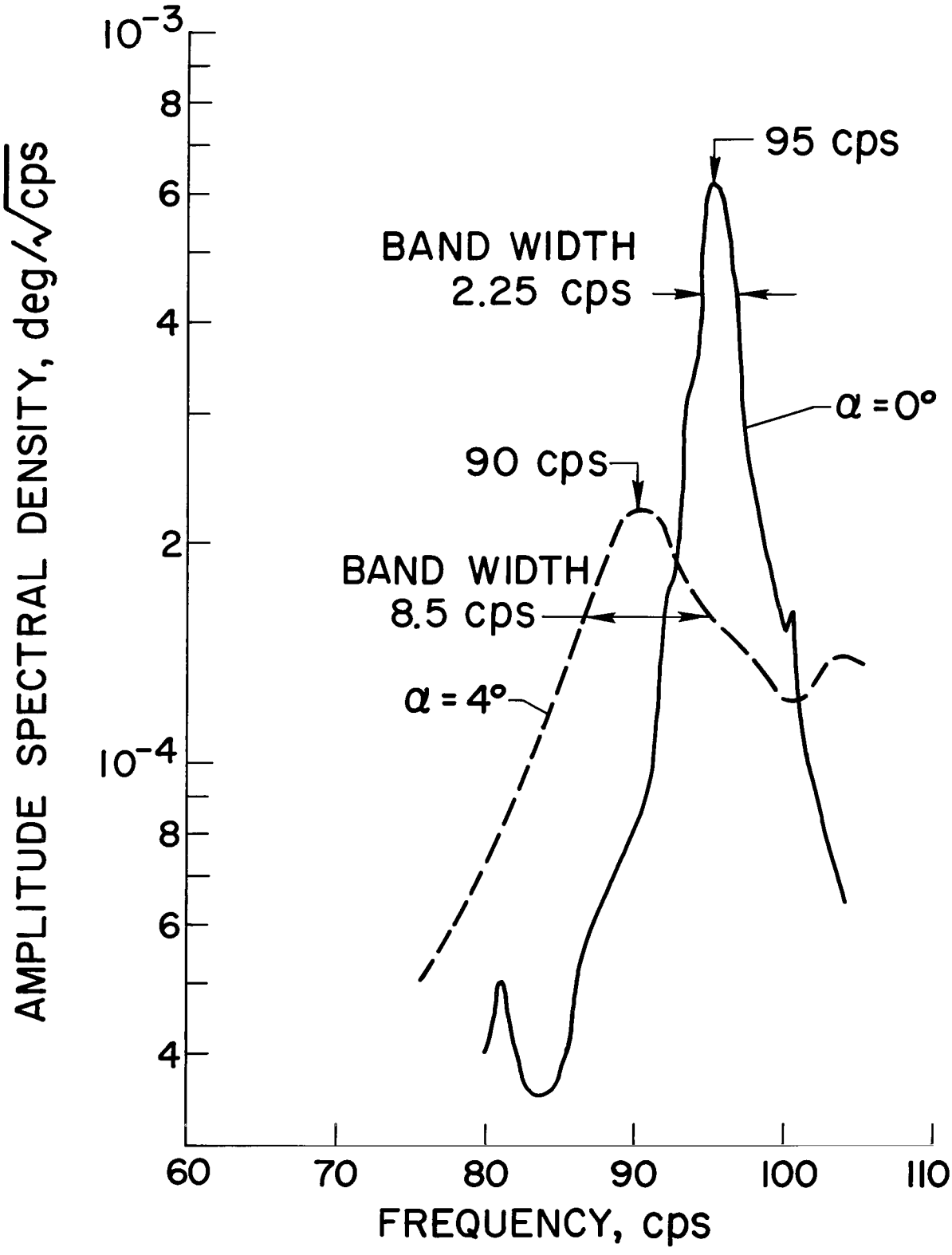

Figure 19.- Spectral densities showing bandwidths at M = 1.51; $\alpha = 0^{\circ}$ and 4°.

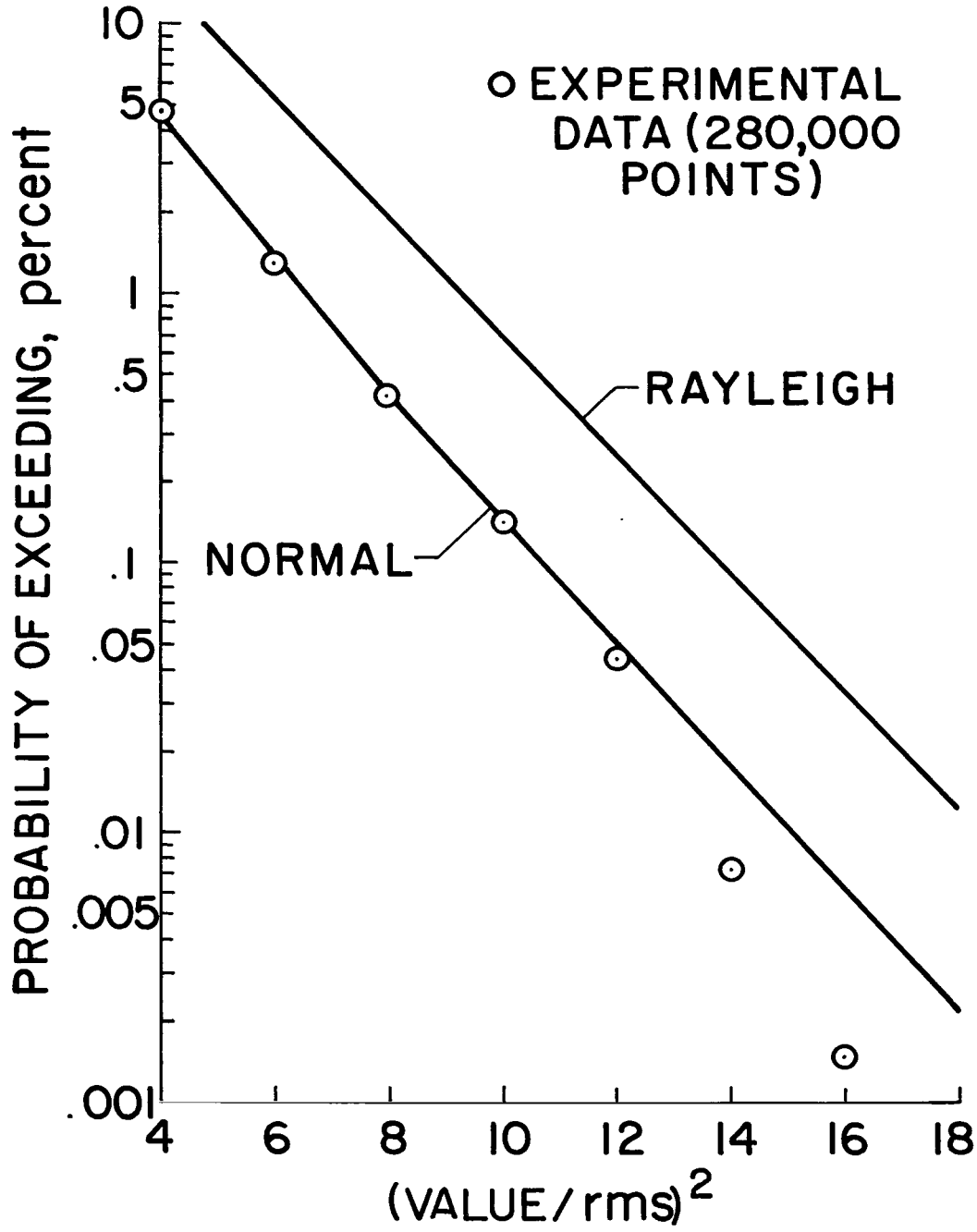

Figure 20.- Distribution of points on time histories.

2/22/85
60

"The aeronautical and space activities of the United States shall be conducted so as to contribute . . . to the expansion of human knowledge of phenomena in the atmosphere and space. The Administration shall provide for the widest practicable and appropriate dissemination of information concerning its activities and the results thereof."

—NATIONAL AERONAUTICS AND SPACE ACT OF 1958

NASA SCIENTIFIC AND TECHNICAL PUBLICATIONS

TECHNICAL REPORTS: Scientific and technical information considered important, complete, and a lasting contribution to existing knowledge.

TECHNICAL NOTES: Information less broad in scope but nevertheless of importance as a contribution to existing knowledge.

TECHNICAL MEMORANDUMS: Information receiving limited distribution because of preliminary data, security classification, or other reasons.

CONTRACTOR REPORTS: Technical information generated in connection with a NASA contract or grant and released under NASA auspices.

TECHNICAL TRANSLATIONS: Information published in a foreign language considered to merit NASA distribution in English.

TECHNICAL REPRINTS: Information derived from NASA activities and initially published in the form of journal articles.

SPECIAL PUBLICATIONS: Information derived from or of value to NASA activities but not necessarily reporting the results of individual NASA-programmed scientific efforts. Publications include conference proceedings, monographs, data compilations, handbooks, sourcebooks, and special bibliographies.

Details on the availability of these publications may be obtained from:

SCIENTIFIC AND TECHNICAL INFORMATION DIVISION

NATIONAL AERONAUTICS AND SPACE ADMINISTRATION

Washington, D.C. 20546